

# Status of Intrinsic Charm

R. Vogt

Lawrence Livermore National Laboratory, Livermore, CA 94551, USA  
Physics and Astronomy Department, UC Davis, Davis, CA 95616, USA



U.S. DEPARTMENT OF  
**ENERGY**

Office of  
Science



Figure 1: This work was performed under the auspices of the U.S. Department of Energy by Lawrence Livermore National Laboratory under Contract DE-AC52-07NA27344, the LLNL-LDRD Program under Projects 21-LW-034 and 23-LW-036 and the HEFTY Collaboration.

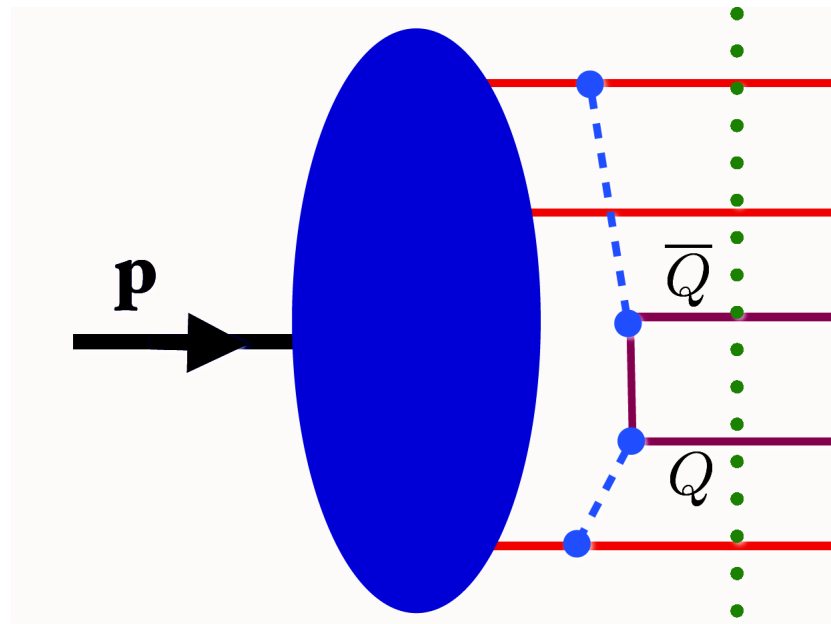
# What is Intrinsic Charm?

Proton wavefunction can be expanded as sum over complete basis of quark and gluon states:  $|\Psi_p\rangle = \sum_m |m\rangle \psi_{m/p}(x_i, k_{T,i}, \lambda_i)$

$|m\rangle$  are color singlet state fluctuations into Fock components  $|uud\rangle, |uudg\rangle \cdots |uudc\bar{c}\rangle$

The intrinsic charm fluctuations can be freed by a soft interaction if the system is probed during the time  $\Delta t = 2p_{\text{lab}}/M_{c\bar{c}}^2$  that the fluctuations exist

Dominant Fock state configurations have minimal invariant mass,  $M^2 = \sum_i m_{T,i}^2/x_i$ , where  $m_{T,i}^2 = k_{T,i}^2 + m_i^2$  is the squared transverse mass of parton  $i$  in the state; corresponds to configurations with equal rapidity constituents



# Brodsky *et al.* Original Intrinsic Charm

Probability distribution of five-particle Fock state of the proton:

$$dP_{ic5} = P_{ic5}^0 N_5 \int dx_1 \cdots dx_5 \int dk_{x1} \cdots dk_{x5} \int dk_{y1} \cdots dk_{y5} \frac{\delta(1 - \sum_{i=1}^5 x_i) \delta(\sum_{i=1}^5 k_{xi}) \delta(\sum_{i=1}^5 k_{yi})}{(m_p^2 - \sum_{i=1}^5 (\hat{m}_i^2/x_i))^2}$$

$i = 1, 2, 3$  are  $u, u, d$  light quarks, 4 and 5 are  $c$  and  $\bar{c}$ ,  $N_t$  normalizes the probability to unity and  $P_{ic}^0$  scales the normalized probability to the assumed intrinsic charm content: 0.1%, 0.31% and 1% are used to represent the range of probabilities assumed previously

The IC cross section is determined from soft interaction scale breaking coherence of the Fock state,  $\mu^2 = 0.1 \text{ GeV}^2$

$$\sigma_{ic}(pp) = P_{ic5} \sigma_{pN}^{\text{in}} \frac{\mu^2}{4\hat{m}_c^2}$$

The cross sections from intrinsic charm are then obtained by multiplying by the normalization factor for the CEM to the  $J/\psi$  while we assume direct correspondence with IC cross section for  $\bar{D}^0$

$$\sigma_{ic}^{\bar{D}}(pp) = \sigma_{ic}(pp) \quad , \quad \sigma_{ic}^{J/\psi}(pp) = F_C \sigma_{ic}(pp)$$

The  $A$  dependence is the same for both  $\bar{D}$  and  $J/\psi$

$$\sigma_{ic}(pA) = \sigma_{ic}(pp) A^\beta$$

where  $\beta = 0.71$  for a proton beam on a nuclear target, as determined by NA3

# Light Cone Intrinsic Charm Quark Distribution

Frame-independent Fock state wavefunction

$$\Psi(\vec{k}_{\perp i}, x_i) = \frac{\Gamma(\vec{k}_{\perp i}, x_i)}{m_h^2 - M^2}$$

Vertex function  $\Gamma$  assumed to be slowly varying so the denominator controls the particle distributions; mean  $k_T^2$  used to calculate the  $x$  distributions

Probability distribution for  $n$ -particle Fock state as a function of  $x$

$$\frac{dP_{ic}}{dx_i \cdots dx_n} = N_n [\alpha_s^2(M_{c\bar{c}})]^2 \frac{\delta(1 - \sum_{i=1}^n x_i)}{(m_h^2 - \sum_{i=1}^n (\hat{m}_i^2/x_i))^2}$$

$N_n$  is a normalization to total probability for each state; heavy quark limit,  $\hat{m}_c, \hat{m}_{\bar{c}} \gg m_h, \hat{m}_q$

$$\frac{dP_{ic}}{dx_i \cdots dx_n} = N_n [\alpha_s^2(M_{c\bar{c}})]^2 \frac{x_c x_{\bar{c}}}{(x_c + x_{\bar{c}})^2} \delta(1 - \sum_{i=1}^n x_i)$$

Finally, in a  $|uudc\bar{c}\rangle$  state,  $n = 5$  and integration over light quarks and  $\bar{c}$  gives

$$c(x) \propto \frac{dP_{ic}(x)}{dx} = \frac{1}{2} N_5 x^2 \left[ \frac{1}{3} (1-x)(1+10x+x^2) + 2x(1+x) \ln x \right]$$

If the intrinsic charm probability is 1%,  $N_5 = 36$

# Other Interpretations of Intrinsic Charm in PDFs

General notion of nonperturbative charm in the parton densities

Radiatively generated charm, also called “extrinsic charm”, is charm parton density determined by the gluon and light quark parameters and DGLAP evolution

Several groups assessed nonperturbative contributions through general global analyses, including coherent treatment of nonzero quark masses in pQCD and experimental inputs that constrain the charm degree of freedom ( $e, \nu$  data from fixed-target DIS with proton and light nuclear targets, HERA, and other data)

One of the first, by Pumplin *et al.* Compared three different scenarios:

- Light cone formalism of Brodsky *et al.*

$$c(x) = \bar{c}(x) = Ax^2[6x(1+x)\ln x + (1-x)(1+10x+x^2)]$$

- Meson/baryon cloud model with  $c(x) \neq \bar{c}(x)$

$$c(x) = Ax^{1.897}(1-x)^{6.095}, \quad \bar{c}(x) = \bar{A}x^{2.511}(1-x)^{4.929}, \quad 0 = \int_0^1 dx [c(x) - \bar{c}(x)]$$

- Charm distribution is sea-like, similar to light flavor sea

$$c(x) = \bar{c}(x) \propto \bar{d}(x) + \bar{u}(x)$$

The NNPDF collaboration has used machine learning with more unstructured parameterizations to look for evidence of large  $x$  charm content

# Potential Experimental Evidence of Intrinsic Charm

A number of experimental hints have been seen, no conclusive results

- Charm structure function,  $F_2^c$ , large at largest  $x$  and highest  $Q^2$  measured (EMC)
- Leading charm asymmetries consistent with intrinsic charm predictions ( $D^-$  over  $D^+$  in  $\pi^-p$  interactions, E791)
- Double  $J/\psi$  production observed at high pair  $x_F$  by NA3
- Forward charm production observed in many fixed-target experiments (WA82, WA89, E791, SELEX and others)
- Proposed explanation of high energy astrophysical neutrino rate at Ice Cube (Brodsky and Laha)
- $Z+c$ -jet measurements at forward rapidity consistent with intrinsic charm (LHCb)

Here some of these results will be shown, typically with some calculations including intrinsic charm

# EMC Measured Excess Events at High $x$ and $Q^2$

Production of charmed particles in 250 GeV  $\mu^+ + \text{Fe}$  interactions

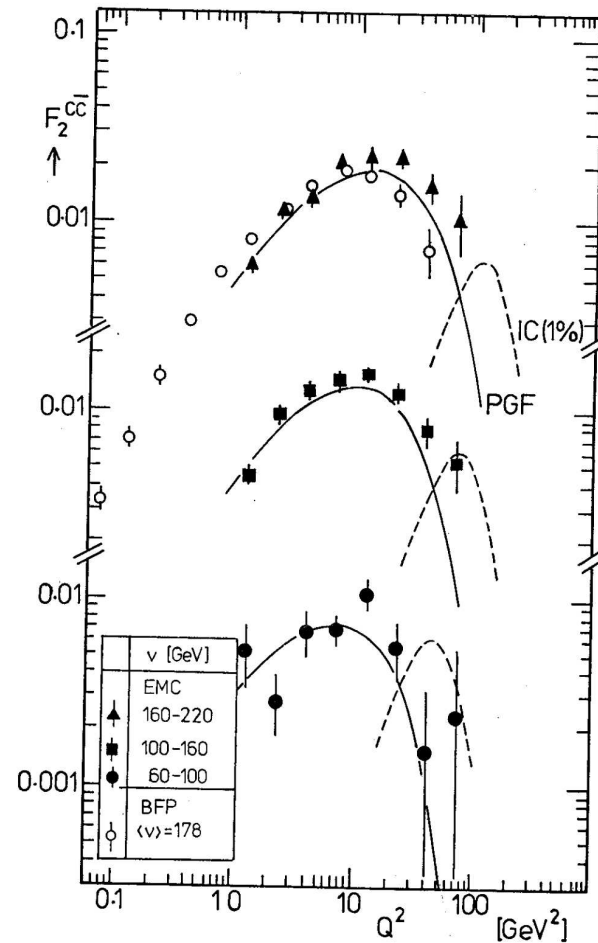


Figure 2: The highest  $\nu = E - E'$  results (corresponding to highest  $x$  bins) shown as a function of  $Q^2$ . The solid curves show charm production by photon-gluon fusion (PGF) and the dashed curves show intrinsic charm (IC). [European Muon Collaboration, *Nucl. Phys. B* **213** (1983) 31.]

# Early PDF Comparison to EMC Data Only

Normalization of extrinsic and intrinsic components kept as free parameters fit to EMC data (Harris, Smith and R.V.)

$$F_2^c(x, Q^2, m_c^2) = \alpha F_2^{c,\text{EC}}(x, Q^2, m_c^2) + \beta F_2^{c,\text{IC}}(x, Q^2, m_c^2)$$

$\alpha$  gives measure of NNLO correction,  $\beta$  is based on a 1% IC normalization

Uncertainties are for 95% confidence level; most significant result is at highest  $\bar{\nu}$

PDF	$\bar{\nu} = 53$ GeV		$\bar{\nu} = 95$ GeV		$\bar{\nu} = 168$ GeV	
	$\alpha$	$\beta$	$\alpha$	$\beta$	$\alpha$	$\beta$
CTEQ3	$0.95 \pm 0.64$	$0.36 \pm 0.58$	$1.20 \pm 0.13$	$0.39 \pm 0.31$	$1.27 \pm 0.06$	$0.92 \pm 0.53$
MRS G	$1.02 \pm 0.69$	$0.34 \pm 0.58$	$1.38 \pm 0.15$	$0.32 \pm 0.32$	$1.47 \pm 0.07$	$0.79 \pm 0.53$
GRV94	$1.15 \pm 0.77$	$0.33 \pm 0.58$	$1.45 \pm 0.16$	$0.34 \pm 0.31$	$1.48 \pm 0.08$	$0.88 \pm 0.53$

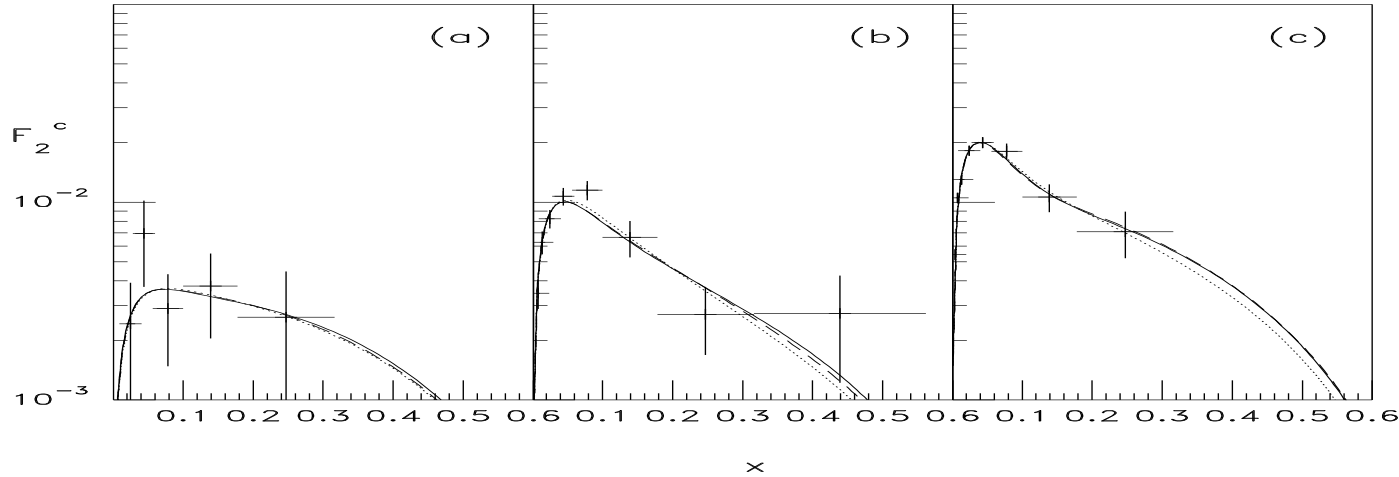


Figure 3: The sum of the EC and IC structure functions, weighted by the parameters  $\alpha$  and  $\beta$ , are compared to the EMC  $F_2^c$  for  $\bar{\nu} = 53$  (a), 95 (b) and 168 (c) GeV. The results are shown for CTEQ3 (solid), MRS G (dotted) and GRV98 (dashed) as a function of  $x$ . (From Harris, Smith and R.V..)



# Forward $\Lambda_c$ Production Observed at CERN ISR

ISR experiment did not cover all phase space, no measured  $\Lambda_c$  at  $x_F \sim 0$

$\Lambda_c(udc)$  can be produced by coalescence from the  $|uudc\bar{c}\rangle$  state

Curves show calculations without IC (dot-dashed) and with (solid and dashed, depending on fragmentation assumed)

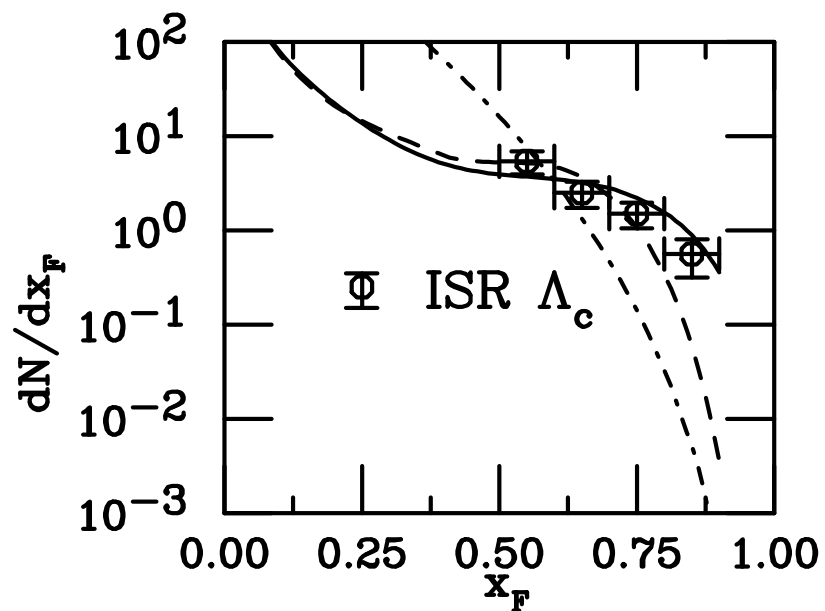


Figure 4: G. Bari *et al.*, Nuovo Cim. A 104, 1787 (1991)

# Double $J/\psi$ Production Observed by CERN NA3

Production of two  $J/\psi$  in  $\pi^-p$  and  $pp$  collisions at fixed-target energies

Single  $J/\psi$  can be produced by  $c\bar{c}$  coalescence from  $|uudc\bar{c}\rangle$  state; for two forward  $J/\psi$ , a  $|uudc\bar{c}\bar{c}\rangle$  state required

Calculations assume only production by intrinsic charm

Pair mass is somewhat higher than mass of two  $J/\psi$ , as expected ( $A_N$ DY experiment at RHIC claimed to observed double  $\Upsilon$  production with pair mass less than  $2m_\Upsilon$ )

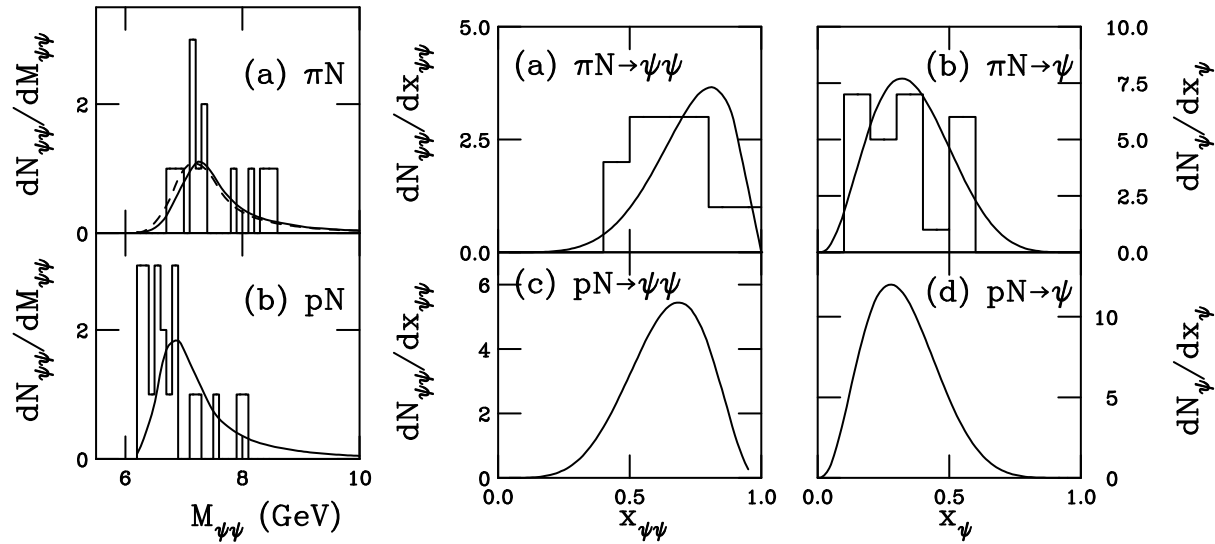


Figure 5: NA3 Collaboration, J. Badier *et al.*, Phys. Lett.B **114** (1982) 457; **158** (1985) 85.

# Charm Hadrons From IC Produced in Forward Region

IC states can either fragment, like normal leading-twist factorization of charm production or coalesce into charm mesons and baryons

Charm hadrons formed by IC coalescence are produced with much higher  $x_F$  than at leading twist, these are leading charm hadrons

Charm hadrons that can't be produced by coalescence from the minimal IC state,  $|\bar{u}dc\bar{c}\rangle$  for  $\pi^-$  and  $|uudc\bar{c}\rangle$  for  $p$  are nonleading

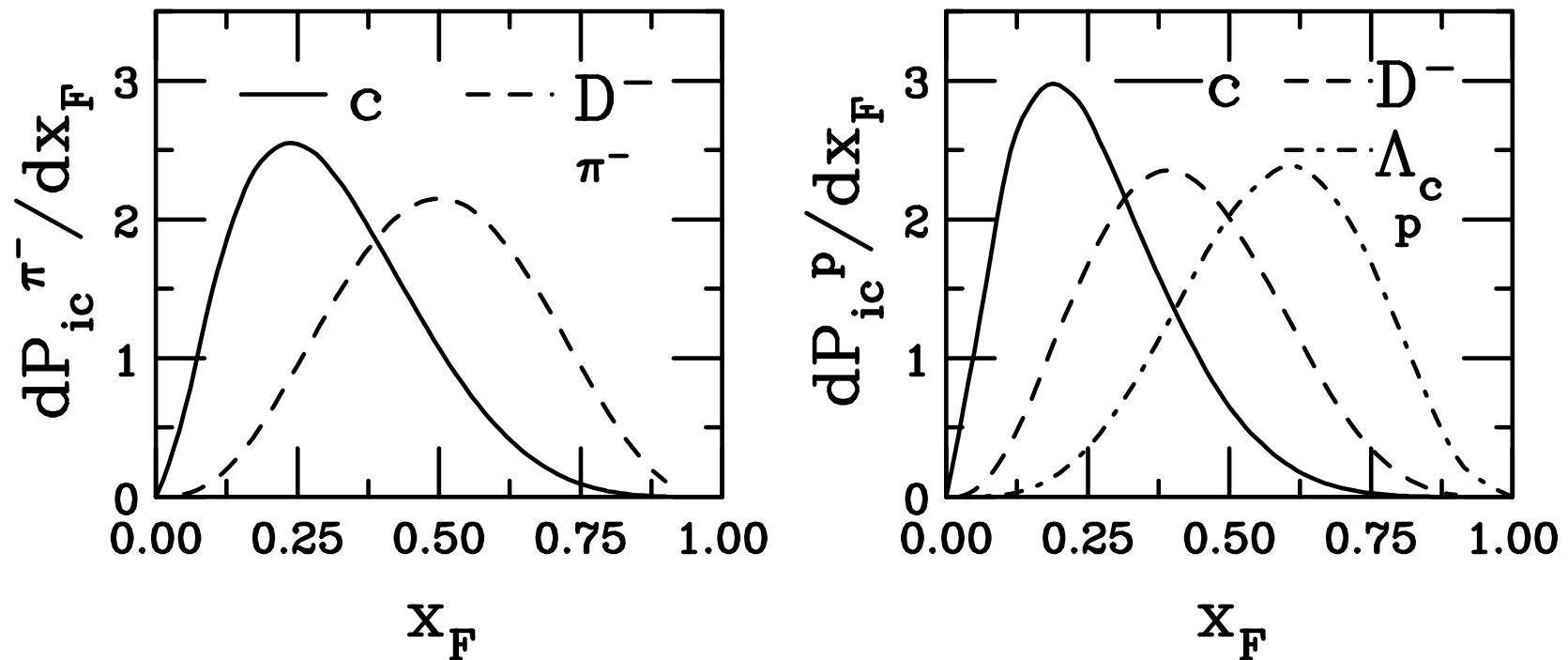


Figure 6: The normalized probability distributions,  $dP_{ic}^n/dx_F$ , for uncorrelated fragmentation and coalescence with a  $\pi^-$  projectile in a 4-particle Fock state (left) and a proton projectile (right). The solid curve in each case is the charm quark distribution. The other curves are the probability distributions for  $D^-$  (dashed) and  $\Lambda_c^+$  (dot-dashed) production by coalescence. [From Gutierrez and RV.]

# Asymmetries Between Leading and Nonleading Charm

Asymmetries mostly observed in fixed target  $\pi^- A$  interactions where  $D^+(\bar{d}c)$  is non-leading and  $D^-(d\bar{c})$  is leading

Should be observable with protons too, fewer measurements with poorer statistics; SMOG device at LHCb now has an asymmetry measurement for  $D^0$  mesons in  $p + \text{Ne}$  interactions at  $\sqrt{s_{NN}} = 68.5 \text{ GeV}$

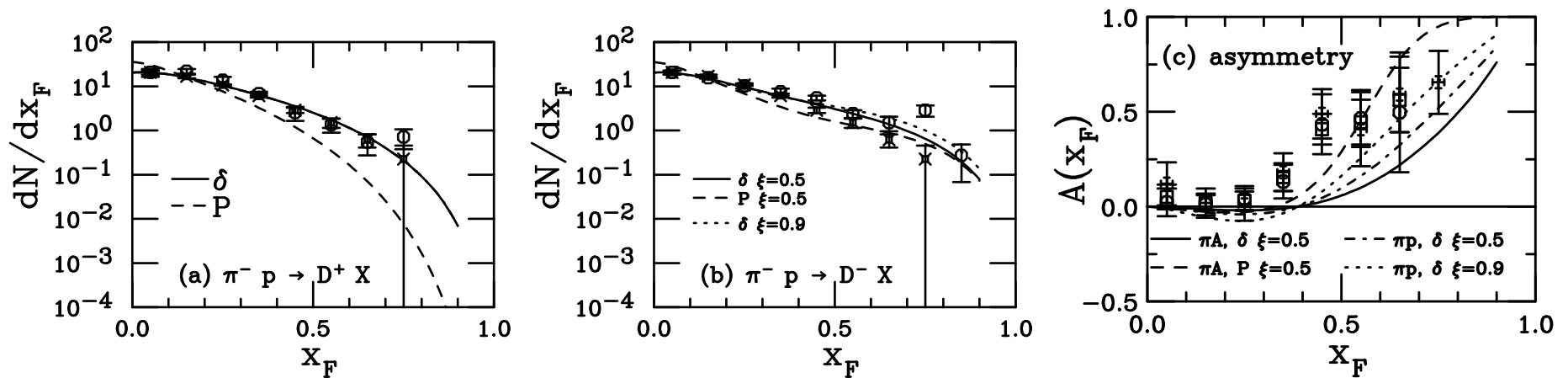


Figure 7: Results for (a) nonleading charm and (b) leading charm distributions in  $\pi^- p$  interactions at 340 GeV and (c) the asymmetry are compared with the WA82 (circles) and E769 (stars) data. The combined asymmetry from both experiments is also shown (squares). The calculations are with GRV LO distributions using delta-function (solid) and Peterson function (dashed) fragmentation with the intrinsic charm contributions to nonleading and leading charm production. The dotted curve in (b) shows the leading  $D$  distribution with  $\xi = 0.9$  (weight factor of coalescence relative to fragmentation). The dot-dashed curve is shows the prediction of fusion with final-state coalescence. In (c), the dashed curve is calculated with the Peterson function and the solid curve with delta-function fragmentation, averaged over nuclear target. The dot-dashed curve uses delta-function fragmentation and a proton target. The dotted curve shows the leading contribution calculated with  $\xi = 0.9$  for a proton target. [From Brodsky and RV.]

# LHCb: Evidence of Intrinsic Charm in $Z + c$ -Jet Events

$Z + c$ -jet ratio to  $Z + \text{all-jet}$  events at  $\sqrt{s} = 13$  TeV is more consistent with calculations including intrinsic charm at high  $y(Z)$ , up to 1% intrinsic charm content

Differences between calculations without intrinsic charm (no IC) and intrinsic charm allowed calculations, either with NNPDF 3.0 including IC or CT14 with a 1% IC content, grows larger with increasing  $y(Z)$

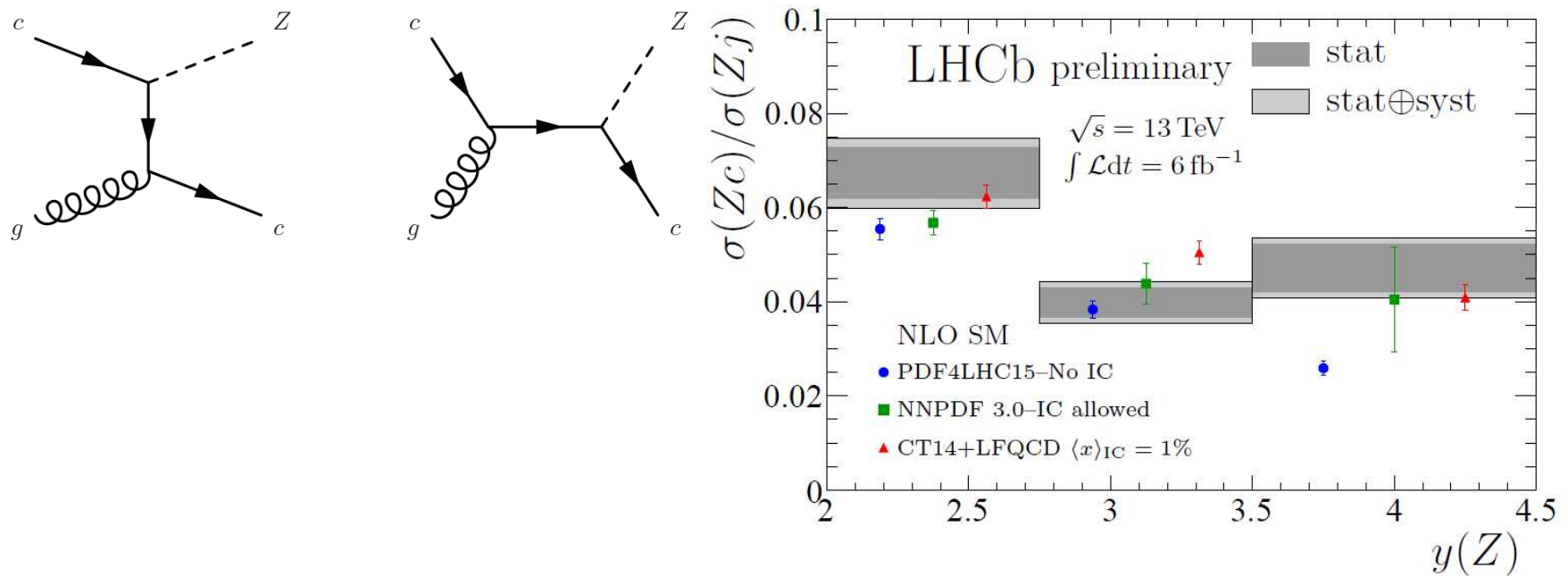


Figure 8: (Left) Leading order diagrams producing  $Z + c$ -jet events. (Right) Ratio of  $Z + c$ -jets to  $Z + \text{all-jet}$  events from LHCb. LHCb data from PRL **128**, 082001 (2022).

# PDF Analyses Including Intrinsic Charm

- Hoffman and Moore calculated intrinsic charm at NLO for EMC only (1983), include mass effects and scale evolution
- Harris, Smith and RV made NLO calculation of extrinsic and intrinsic charm at NLO, 1990, found approximate  $(0.86 \pm 0.60)\%$  contribution at highest  $Q^2$  fitting EMC data only
- Pumplin *et al.* made first global analysis of proton PDFs (2007) including intrinsic charm assuming BHPS and meson-cloud model ( $c(x) \neq \bar{c}(x)$ ) shapes as well as 'sea-like' with the same shape as radiatively-generated extrinsic charm, the CTEQ6.6C sets
- Dulat *et al.*, based on CT10 NNLO PDFs, included DIS and hadroproduction, found  $\langle x \rangle_{c+\bar{c}}(Q_0^2) \leq 0.025$  for BHPS,  $\leq 0.015$  for sea-like
- Jimenez-Delgado *et al.*, included lower energy data and more stringent tolerance than Dulat, found  $\langle x \rangle_{c+\bar{c}} < 0.1\%$  at  $5\sigma$  level (agree with Dulat with same tolerance)
- NNPDF Collaboration (Ball *et al.*) compared global analyses with “perturbative charm” (extrinsic) and “fitted charm” (intrinsic charm), concluded that charm at low  $x$  is perturbative but, at low scales and high  $x$ , the data support an intrinsic component

# NNPDF4: Evidence for Intrinsic Charm I

Parameterize the 4 flavor number scheme (4FNS) freely and fit charm in a global analysis, matching to 3FNS can be inverted to obtain the intrinsic charm component if the 3FNS contribution does not vanish, as with no intrinsic charm

Extracted 3FNS charm distribution shows a valence-like structure at large  $x$ , with a peak around  $x \sim 0.4$ ; no radiatively generated charm in this region

Missing higher order uncertainties (MHOU) estimated by transforming from 4FNS PDF at NNLO at N<sup>3</sup>LO; peak does not change but uncertainties for  $x < 0.2$  become very large (light blue band is PDFU + MHOU added in quadrature)

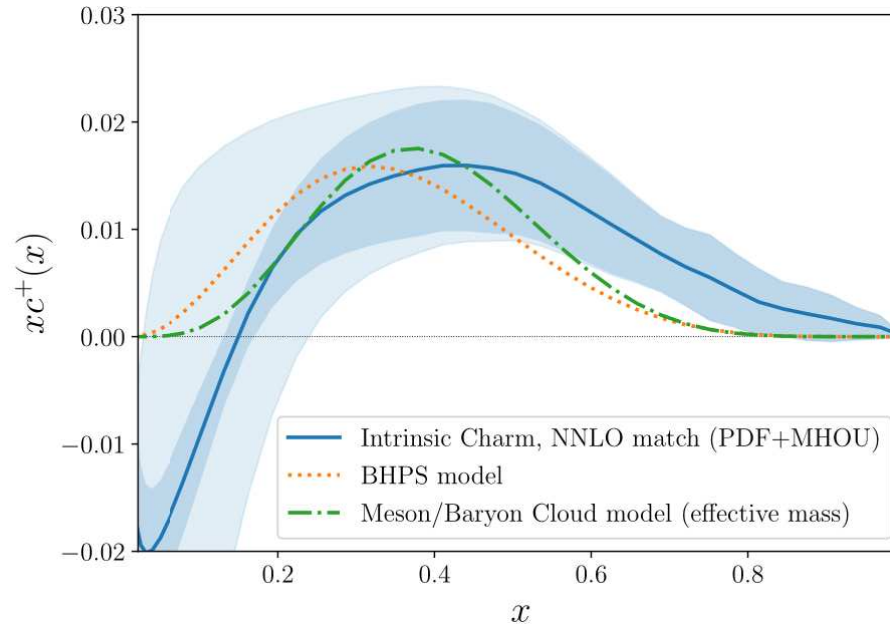


Figure 9: Dark Blue band shows the extracted intrinsic charm distribution with PDF uncertainties only, based on the NNPDF4.0 PDFs; light blue band includes MHOU; orange line is the Brodsky *et al.* distribution and the dark green line is the charm distribution from the meson/baryon cloud model. [NNPDF Collaboration, Nature **608** (2022) 483–487].

# NNPDF4: Evidence for Intrinsic Charm II

NNPDF Collaboration studied the stability of their results by looking at the dependence on the datasets used in the analysis; the parameterization basis (evolution basis – linear combinations of  $q$  and  $\bar{q}$  distributions – or individual PDF basis); charm quark mass dependence

The charm momentum fraction (probability for intrinsic charm) is between 0.5% and 0.8%, albeit with large combined uncertainties, particularly from the MHOUS. Statistical significance reaches 3 sigma with LHCb  $Z + c$ -jet and EMC data are included (either and both)

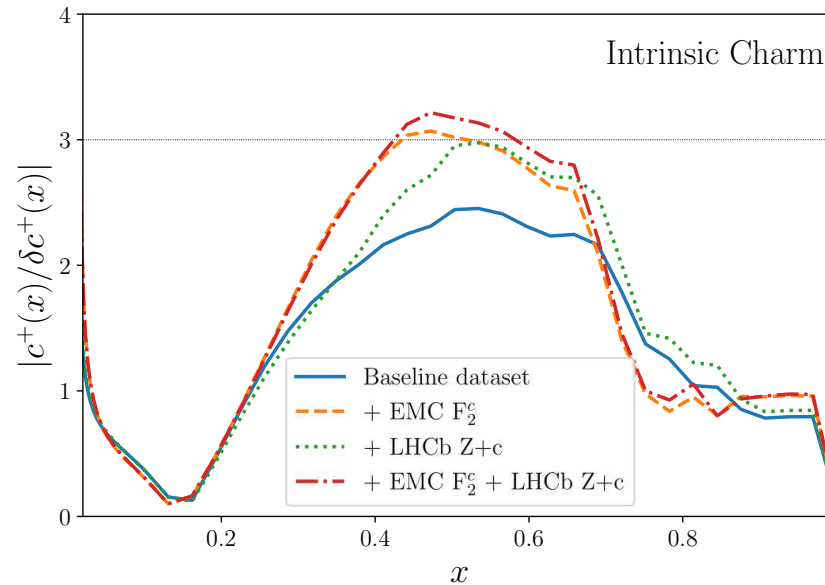


Figure 10: Statistical significance of the results for the baseline dataset (without the  $Z + c$ -jet and EMC data) and adding in one or both of these higher  $x$  datasets. [NNPDF Collaboration, Nature **608** (2022) 483–487.]



# Not So Fast: CT18 (Guzzi *et al.*) I

Argue that fitted charm PDF that parameterizations of  $xc(x)$  extracted near threshold are only approximation because they may absorb contributions unrelated to IC and that without a way to connect the fitted charm in PDF analyses to IC models it is impossible to guarantee that the resulting IC is a universal component of the proton wavefunction

Most available DIS measurements are low  $x$  and thus not very sensitive to IC; the NNLO  $Z + c$ -jet calculation has not been incorporated into global analyses so they claim these data are not sufficiently accurate to discriminate between IC models

Augmented CT18 with 4 variations of fitted charm and underlying IC model: BHPS (standard IC with either CT18 NNLO or CT18X NNLO) and MCM (meson cloud model with  $p \equiv \overline{D}\Lambda_c$  and either confining or effective mass quark models)

All four models give low probability for intrinsic charm (related to first moment,

$$\langle x \rangle(Q_0^2) \sim 0.004 - 0.006 \quad (1)$$

Claim that NNPDF “evidence” would also equally well allow a nearly zero IC contribution with more comprehensive sampling and that their uncertainties are underestimated (they also note that otherwise the frameworks and procedures are similar for NNPDF and CT18)

# Not So Fast: CT18 (Guzzi *et al.*) II

Left side shows the four variations of fitted charm used for the analysis, all peaking at higher  $x$  than perturbatively generated charm

Figures on the right show the difference in the LHCb  $Z + c$ -jet analysis based on whether or not the generator used with the PDFs includes parton showering or not; including showering enhances the intrinsic charm (difference between Powheg and MCFM); with MCFM and more recent PDF sets, the difference calculations do not match the data as well

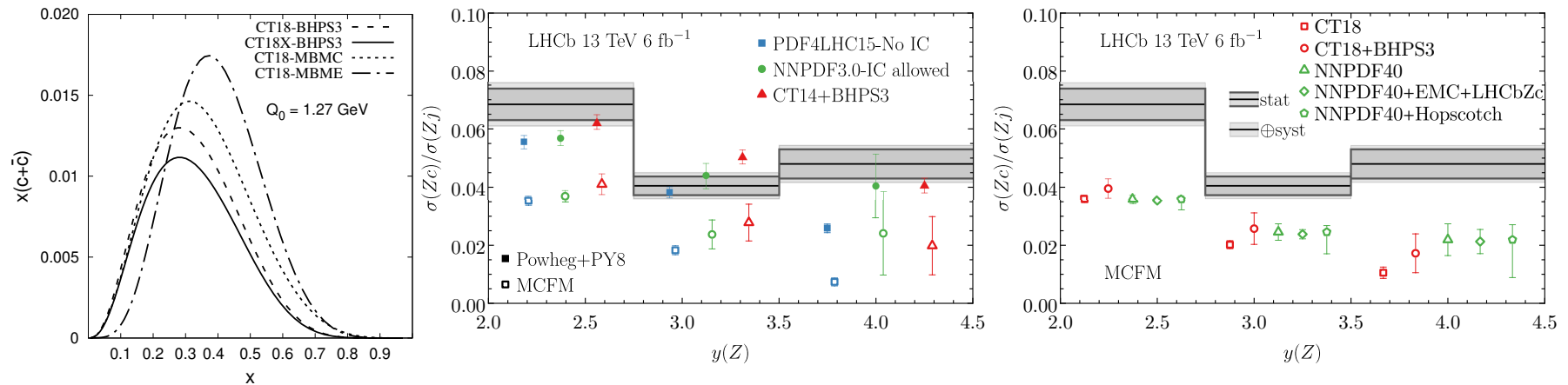


Figure 11: CT18, Guzzi *et al.*, arXiv:2211.01387.

# IC Potentially Easier to Measure in Fixed-Target Experiments

As  $\sqrt{s_{NN}}$  increases, the intrinsic charm rapidity distribution is moved further away from midrapidity, at collider energies it is inaccessible to most forward detectors

The  $p_T$  distributions are shown with the rapidity range is restricted to  $0 < y < 1$ , green curve shows integration over all  $y$ ; if  $y$  acceptance at higher  $y$ , more of the IC  $p_T$  distribution is captured

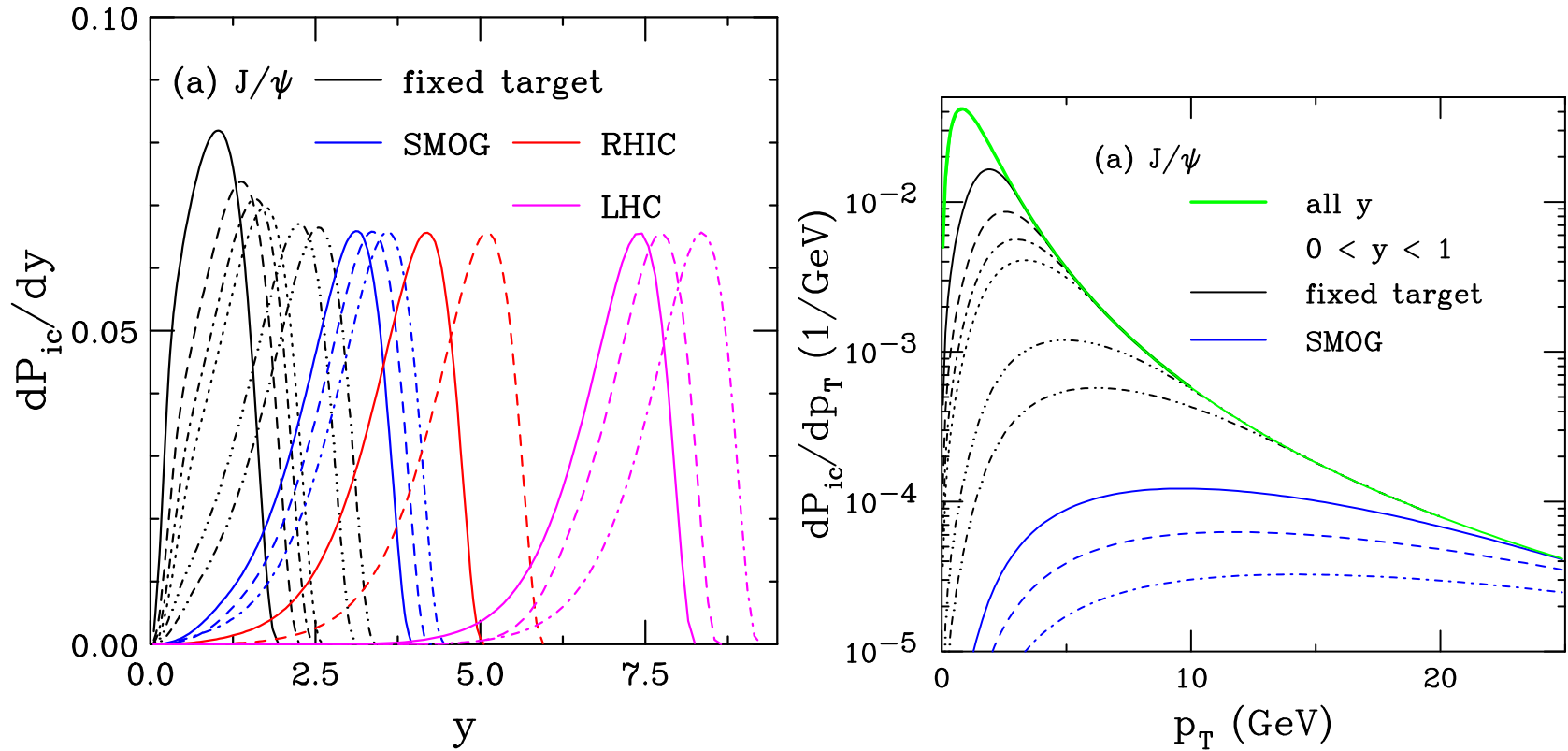


Figure 12: The probability distributions for  $J/\psi$  production from a five-particle proton Fock state as a function of  $y$  (left) and  $p_T$  (right). The rapidity distributions are shown for  $\sqrt{s} = 8.8$  GeV to 13 TeV. (Right) The results are shown for all rapidity in the solid green curve. Results for restricting the rapidity range to  $0 < y < 1$  are shown for  $p_{lab} = 40, 80$  and  $120$  GeV by the solid black, dashed blue and dot-dashed red respectively.

# Recent and Forthcoming Fixed-Target Experiments Ideal for IC Studies

Many previous experiments studied  $J/\psi$  production off nuclear targets at proton beam energies from 158 to 920 GeV, several used to get a baseline for  $A + A$  collisions; those that covered large  $x_F$  saw a larger suppression of production off nuclear targets at higher  $x_F$

**SeaQuest:** Took data with a 120 GeV proton beam on  $p$ ,  $d$ ,  $C$ ,  $Fe$ , and  $W$  targets, covered forward region,  $0.4 < x_F < 0.95$  and  $p_T < 2.3$  GeV;  $J/\psi$  data not published yet but should report nuclear suppression factor,  $pA/pd$

**SMOG:** Gas jet target in LHCb,  $J/\psi$  and  $D^0$  measured at backward rapidity in the fixed-target center of mass, data so far at:  $p + Ne$  at  $\sqrt{s_{NN}} = 68.5$  GeV;  $p + He$  at  $\sqrt{s_{NN}} = 86.6$  GeV; and  $p + Ar$  at  $\sqrt{s_{NN}} = 110.4$  GeV

**NA60+:** proton beams at  $p_{lab} = 40, 80, \text{ and } 120$  GeV, nuclear targets from  $Be$  to  $Pb$

Calculations and comparison to data in the following from R. Vogt, arXiv:2101.02858, Phys. Rev. C 103, 035204 (2021); arXiv:2207.04347, Phys. Rev. C 106, 025201 (2022); arXiv:2304.03451, Phys. Rev. C to be published

# Compare to Calculations Including Perturbative and Nonperturbative Charm

$J/\psi$  and  $D$  meson production included

The production cross sections are calculated with a combination of perturbative QCD and intrinsic charm contributions; in  $p + p$  collisions:

$$\begin{aligned}\sigma_{pp}^{\overline{D}} &= \sigma_{\text{OHF}}(pp) + \sigma_{\text{ic}}^{\overline{D}}(pp) \\ \sigma_{pp}^{J/\psi} &= \sigma_{\text{CEM}}(pp) + \sigma_{\text{ic}}^{J/\psi}(pp)\end{aligned}$$

The  $D$  meson and  $J/\psi$  cross sections are computed at NLO in the color evaporation model for  $p + p$  and  $p + A$  interactions;  $\sigma_{\text{ic}}$  is the intrinsic charm cross section using Brodsky *et al.* “flavor” of IC

In  $p + A$  collisions:

$$\begin{aligned}\sigma_{pA}^{\overline{D}} &= \sigma_{\text{OHF}}(pA) + \sigma_{\text{ic}}^{\overline{D}}(pA) \\ \sigma_{pA}^{J/\psi} &= \sigma_{\text{CEM}}(pA) + \sigma_{\text{ic}}^{J/\psi}(pA)\end{aligned}$$

# Charm Production in Perturbative QCD

The perturbative QCD cross section at NLO for open heavy flavor and quarkonium is

$$\sigma_{\text{OHF}}(pp) = \sum_{i,j} \int_{4m^2}^{\infty} d\hat{s} \int dx_1 dx_2 F_i^p(x_1, \mu_F^2, k_{T1}) F_j^p(x_2, \mu_F^2, k_{T2}) \hat{\sigma}_{ij}(\hat{s}, \mu_F^2, \mu_R^2) ,$$

$$\sigma_{\text{CEM}}(pp) = F_C \sum_{i,j} \int_{4m^2}^{4m_H^2} ds \int dx_1 dx_2 F_i^p(x_1, \mu_F^2, k_{T1}) F_j^p(x_2, \mu_F^2, k_{T2}) \hat{\sigma}_{ij}(\hat{s}, \mu_F^2, \mu_R^2)$$

Parton densities factorized into longitudinal (CT10) and a  $k_T$ -dependent component to implement  $k_T$  broadening a la low  $p_T$  resummation; Peterson fragmentation with parameter modified to agree with FONLL included for open charm

$$F^p(x, \mu_F^2, k_T) = f^p(x, \mu_F^2) G_p(k_T)$$

$$G_p(k_T) = \frac{1}{\pi \langle k_T^2 \rangle_p} \exp(-k_T^2 / \langle k_T^2 \rangle_p)$$

$$\langle k_T^2 \rangle_p = \left[ 1 + \frac{1}{n} \ln \left( \frac{\sqrt{s_{NN}}(\text{GeV})}{20 \text{ GeV}} \right) \right] \text{ GeV}^2$$

$\langle k_T^2 \rangle_p$  broadening assumed energy dependent,  $n = 12$  from  $J/\psi$  data

$\langle k_T^2 \rangle_p$  increases slowly from less than 1  $\text{GeV}^2$  at  $p_{\text{lab}} = 120 \text{ GeV}$  to 1.14  $\text{GeV}^2$  at  $\sqrt{s_{NN}} = 110.4 \text{ GeV}$ , the highest SMOG energy

# $J/\psi$ $p + p$ distributions as a function of $y$ and $p_T$ : With and Without Intrinsic Charm

The strong energy dependence of the intrinsic charm contribution is evident; the pQCD contribution is overwhelmed at low energies but IC becomes negligible except for very forward rapidity at higher energies

Restricting the calculated  $p_T$  distributions to midrapidity significantly reduces the intrinsic charm contribution at low  $p_T$ , even for the lowest energies

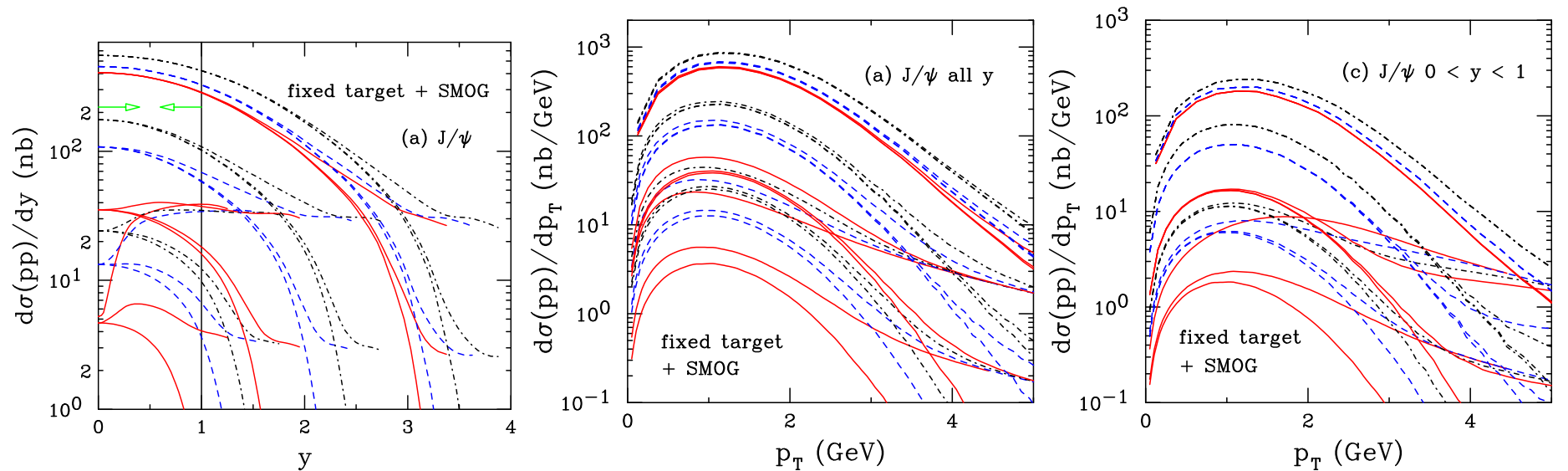


Figure 13: The combined distributions for  $J/\psi$  as a function of rapidity (left) and  $p_T$  (center and right), including both the perturbative QCD contribution and intrinsic charm from a  $|uudc\bar{c}\rangle$  state. The calculated  $p_T$  distributions are integrated over all rapidity (middle) but limited to  $0 < y < 1$  (right). Three curves are shown for each energy: no intrinsic charm (pQCD only);  $P_{ic5}^0 = 0.1\%$ ; and  $P_{ic5}^0 = 1\%$ . The results are shown for fixed-target and SMOG energies, starting from  $p_{lab} = 40$  GeV (red solid), 80 GeV (blue dashed), 120 GeV (black dot-dashed), 158 GeV (red solid), 450 GeV (blue dashed), 800 GeV (black dot-dashed),  $\sqrt{s} = 69$  GeV (solid red), 87.7 GeV (blue dashed) and 110.4 GeV (black dot-dashed). On the left, the vertical line with the green arrows shows the assumed rapidity acceptance of  $0 < y < 1$ .

# $J/\psi$ Distributions in $p + p$ at SMOG Energies

Cross section uncertainties calculated using same mass and scale parameters

CEM normalization  $F_C$  set by comparison to total cross section, same value of  $F_C$  is used for all uncertainty sets and all energies

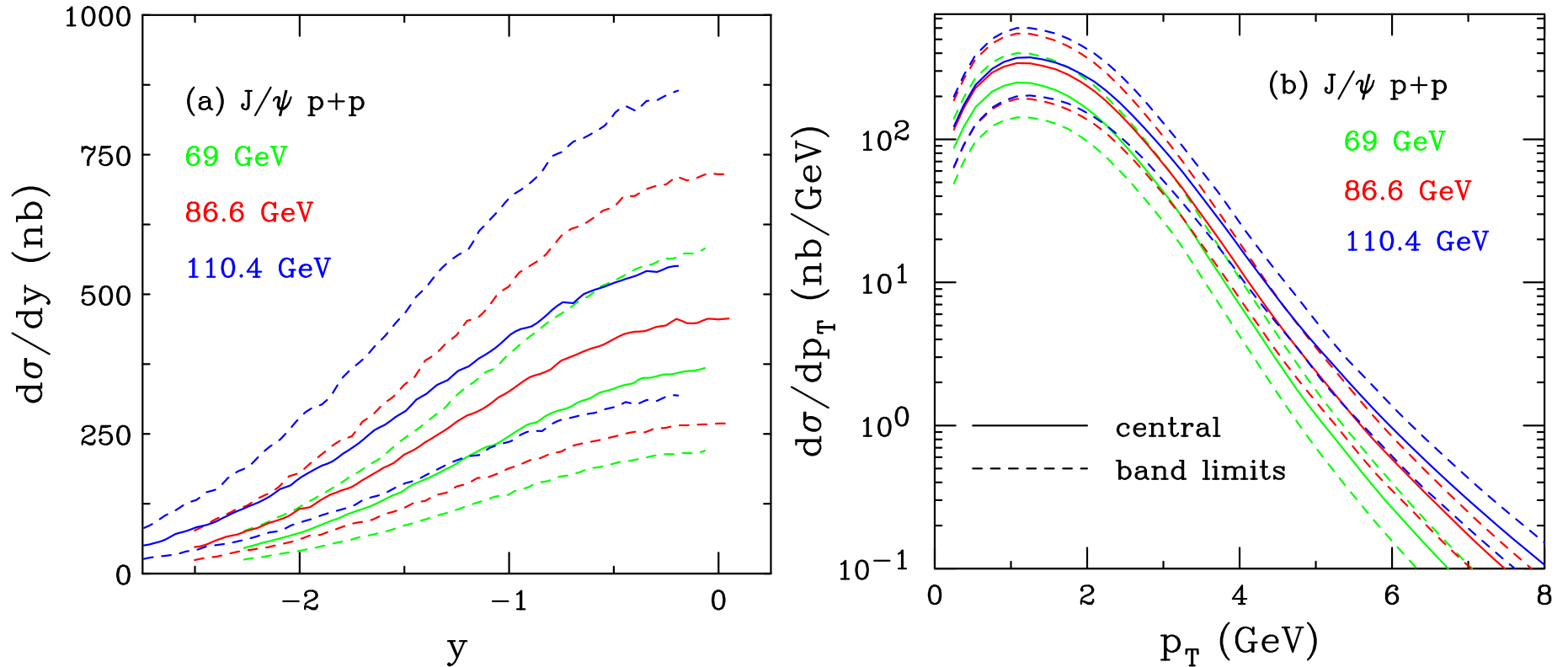


Figure 14: The  $J/\psi$  production cross sections in the CEM in  $p + p$  collisions at  $\sqrt{s} = 68.5$  (green), 86.6 (red), and 110.4 GeV (blue) as a function of rapidity (a) and  $p_T$  (b), in the SMOG fixed-target acceptance, is shown. The solid curves show the central values while the dashed curves outline the upper and lower limits of the uncertainty band.



# $\bar{D}$ $p + p$ distributions as a function of $y$ and $p_T$ : With and Without Intrinsic Charm

Results are similar for  $\bar{D}$  as for  $J/\psi$ , main difference is that the  $\bar{D}$  distributions are somewhat broader while the  $p_T$  distributions have a slightly lower average  $p_T$

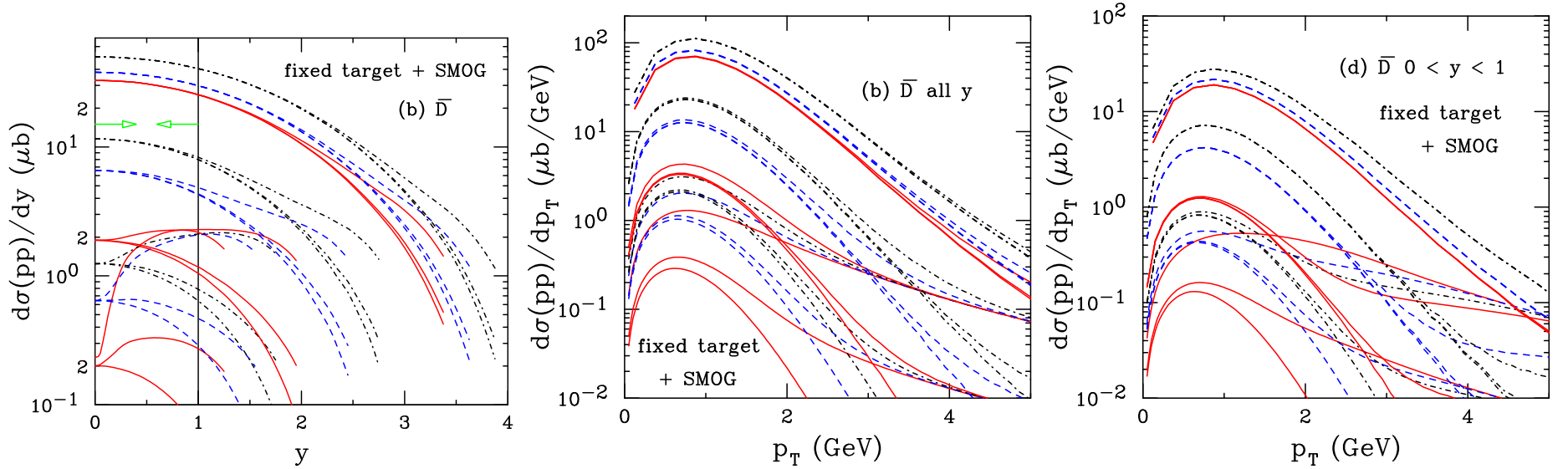


Figure 15: The combined distributions for  $\bar{D}$  mesons as a function of rapidity (left) and  $p_T$  (center and right), including both the perturbative QCD contribution and intrinsic charm from a  $|uudc\bar{c}\rangle$  state. The calculated  $p_T$  distributions are integrated over all rapidity (middle) but limited to  $0 < y < 1$  (right). Three curves are shown for each energy: no intrinsic charm (pQCD only);  $P_{ic5}^0 = 0.1\%$ ; and  $P_{ic5}^0 = 1\%$ . The results are shown for fixed-target and SMOG energies, starting from  $p_{\text{lab}} = 40$  GeV (red solid), 80 GeV (blue dashed), 120 GeV (black dot-dashed), 158 GeV (red solid), 450 GeV (blue dashed), 800 GeV (black dot-dashed),  $\sqrt{s} = 69$  GeV (solid red), 87.7 GeV (blue dashed) and 110.4 GeV (black dot-dashed). On the left, the vertical line with the green arrows shows the assumed rapidity acceptance of  $0 < y < 1$ .

# $D$ Distributions in $p + p$ at SMOG Energies

Uncertainty bands defined by  $(m, \mu_F/m_T, \mu_R/m_T) = (1.27 \pm 0.09 \text{ GeV}, 2.1_{-0.85}^{+2.55}, 1.6_{-0.12}^{+0.11})$ ;  $\mu_F$ , factorization scale, and  $\mu_R$ , renormalization scale, defined relative to pair transverse mass:  $\mu_{F,R} \propto m_T = \sqrt{m^2 + p_T^2}$  where  $p_T^2 = 0.5(p_{T_Q}^2 + p_{T_{\bar{Q}}}^2)$

Scale uncertainties set by  $\{(\mu_F/m_T, \mu_F/m_T)\} = \{(C, C), (H, H), (L, L), (C, L), (L, C), (C, H), (H, C)\}$  (Mass uncertainties dominate.)

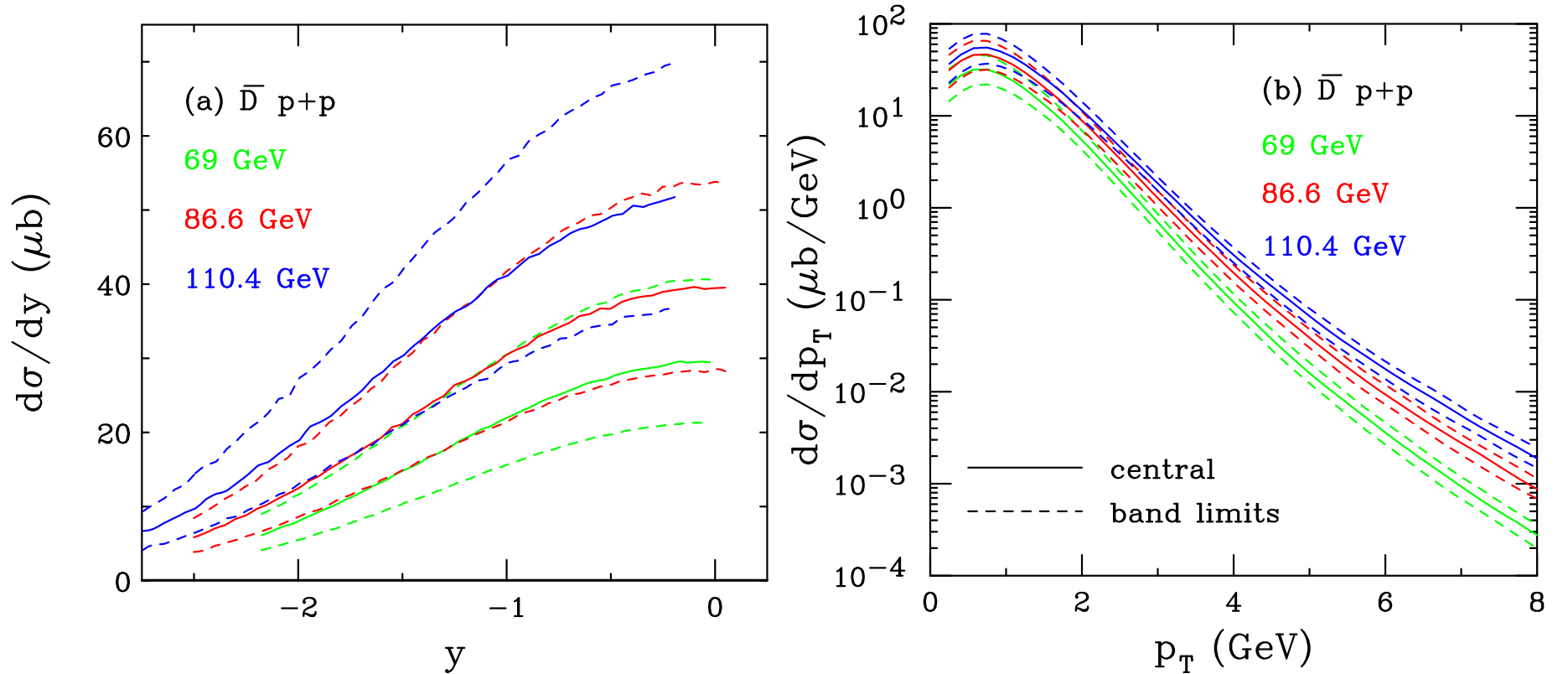


Figure 16: (Color online) The NLO  $\bar{D}^0$  production cross sections in  $p + p$  collisions at  $\sqrt{s} = 68.5$  (green), 86.6 (red), and 110.4 GeV (blue) as a function of rapidity (a) and  $p_T$  (b), in the SMOG fixed-target acceptance, are shown. The solid curves show the central values while the dashed curves outline the upper and lower limits of the uncertainty band.

# For Nuclear Targets, Include Cold Nuclear Matter Effects

Production cross section in a  $pA$  collision is

$$\sigma_{pA} = \sigma_{\text{CEM}}(pA) = S_A^{\text{abs}} F_C \sum_{i,j} \int_{4m^2}^{4m_H^2} ds \int dx_1 dx_2 F_i^p(x_1, \mu_F^2, k_T) F_j^A(x_2, \mu_F^2, k_T) \hat{\sigma}_{ij}(\hat{s}, \mu_F^2, \mu_R^2)$$

Survival probability for absorption of a (proto)charmonium state in nuclear matter:

$$\begin{aligned} \sigma_{pA} = \sigma_{pN} S_A^{\text{abs}} &= \sigma_{pN} \int d^2b \int_{-\infty}^{\infty} dz \rho_A(b, z) S^{\text{abs}}(b) \\ &= \sigma_{pN} \int d^2b \int_{-\infty}^{\infty} dz \rho_A(b, z) \exp \left\{ - \int_z^{\infty} dz' \rho_A(b, z') \sigma_{\text{abs}}(z' - z) \right\} \end{aligned}$$

The absorption cross section is assumed constant. Prior fixed-target experiments extracted an effective absorption cross section from  $A^\alpha$  analysis with  $\alpha = 1 - 9\sigma_{\text{abs}}/(16\pi r_0^2)$  assuming no other nuclear effects ( $J/\psi$  only)

Nuclear parton densities

$$\begin{aligned} F_j^A(x_2, \mu_F^2, k_T) &= R_j(x_2, \mu_F^2, A) f_j(x_2, \mu_F^2) G_A(k_T) \\ F_i^p(x_1, \mu_F^2, k_T) &= f_i(x_1, \mu_F^2) G_p(k_T) \end{aligned}$$

$G_A(k_T)$  includes increased broadening in the nuclear target ( $A > 2$ )

# $k_T$ Broadening in Nuclei

$k_T$  broadening in nuclei may be enhanced through multiple scattering in the target; to implement enhanced broadening, a larger value of  $\langle k_T^2 \rangle$  is used for nuclear targets

$$\langle k_T^2 \rangle_A = \langle k_T^2 \rangle_p + \delta k_T^2$$

$\delta k_T^2$  gives strength of broadening

$$\delta k_T^2 = (\langle \nu \rangle - 1) \Delta^2(\mu)$$

The broadening strength depends on the interaction scale:

$$\Delta^2(\mu) = 0.225 \frac{\ln^2(\mu/\text{GeV})}{1 + \ln(\mu/\text{GeV})} \text{GeV}^2 \quad \mu = 2m_c$$

Strength also depends on number of scatterings proton undergoes passing through nuclear target,  $\langle \nu \rangle - 1$

$$\langle \nu \rangle = \sigma_{pp}^{\text{in}} \frac{\int d^2b T_A^2(b)}{\int d^2b T_A(b)} = \frac{3}{2} \rho_0 R_A \sigma_{pp}^{\text{in}}$$

$T_A$  is the nuclear profile function, here  $\rho_0 = 0.16/\text{fm}^3$ ,  $R_A = 1.2A^{1/3}$ , and the inelastic  $p + p$  cross section is  $\sigma_{pp}^{\text{in}} \sim 30$  mb for the energies considered here

**Example for SMOG:** for helium, neon, and argon targets,  $\delta k_T^2 = 0.05$ , **0.15**, and **0.22**  $\text{GeV}^2$  respectively, giving an average broadening of  $\langle k_T^2 \rangle_A = 1.17$ , **1.25**, and **1.36**  $\text{GeV}^2$  for  $p + \text{He}$ ,  $p + \text{Ne}$  and  $p + \text{Ar}$  respectively

# Nuclear Modification of the Parton Densities

EPPS16 nuclear parton density modifications differentiate between  $u$  and  $d$  valence quarks and all sea quarks; 20 parameters give 40 error sets + 1 central set

Uncertainties are determined by calculating cross section for each  $A$  with all error sets, adding differences around central set for each parameter in quadrature

Lower energies probe higher  $x$ , for  $0 < y < 1$ , the momentum fraction in the nucleus is in the antishadowing and EMC regions (see right-hand plot)

$$f_j^A(x_2, \mu_F^2) = R_j(x_2, \mu_F^2, A) f_j^p(x_2, \mu_F^2)$$

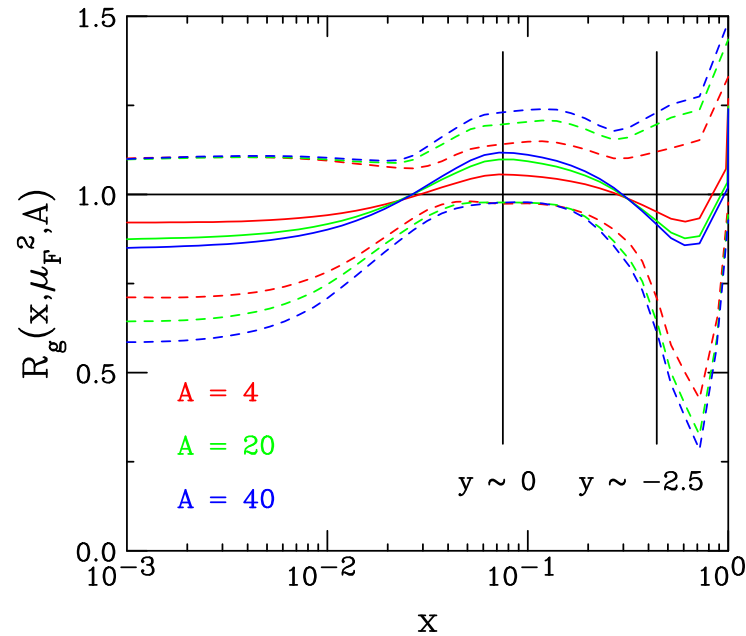


Figure 17: (Color online) The EPPS16 ratios, with uncertainties, are shown at the scale of the  $J/\psi$  mass for gluons as a function of momentum fraction  $x$ . The central set is denoted by the solid curves while the dashed curves give the upper and lower limits of the uncertainty bands. The results are given for  $A = 4$  (red), 20 (green), and 40 (blue). The vertical lines indicate the  $x$  range of the SMOG device,  $0.075 < x < 0.44$ .

# Energy Dependence of $\sigma_{\text{abs}}^{J/\psi}$

At midrapidity, systematic decrease of  $\sigma_{\text{abs}}^{J/\psi}$  with  $\sqrt{s_{NN}}$ , independent of shadowing, trend continues at RHIC and above

$\sigma_{\text{abs}}^{J/\psi}(y_{\text{cms}} = 0)$  at 158 GeV is significantly larger than that measured at 450 GeV

Absorption cross section can be  $\sim 9$  mb at lowest energies,  $\sigma_{\text{abs}} = 4, 3.5,$  and  $3$  mb are used at  $\sqrt{s_{NN}} = 68.5, 86.6$  and  $110.4$  GeV; negligible absorption assumed for LHC collider energies

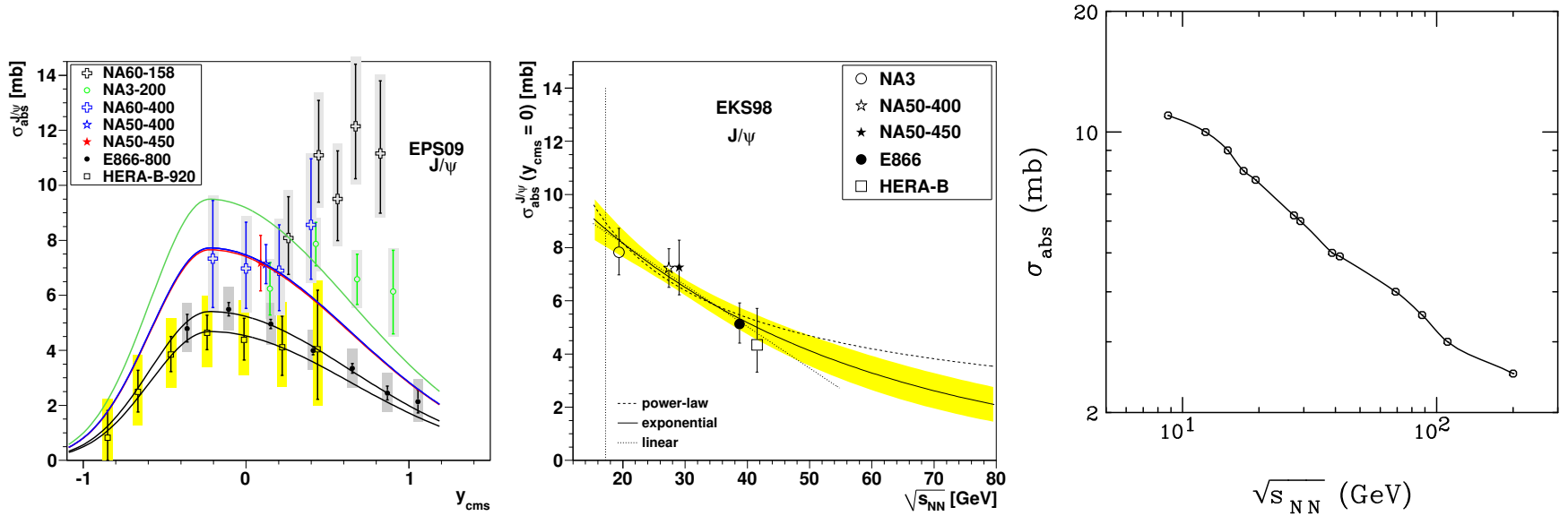


Figure 18: Left: Dependence of  $\sigma_{\text{abs}}^{J/\psi}$  on  $y_{\text{cms}}$  for all available data sets including EPS09 shadowing. The shape of the curves is fixed by the E866 and HERA-B data. [Lourenço, RV, Wöhri] Middle: The extracted energy dependence of  $\sigma_{\text{abs}}^{J/\psi}$  at midrapidity for power law (dashed), exponential (solid) and linear (dotted) approximations to  $\sigma_{\text{abs}}^{J/\psi}(y = 0, \sqrt{s_{NN}})$  using the EKS98 shadowing parameterization with the CTEQ61L parton densities. The band around the exponential curve indicates the uncertainty in the extracted cross sections at  $x_F \sim 0$  from NA3, NA50 at 400 and 450 GeV, E866 and HERA-B. The vertical dotted line indicates the energy of the Pb+Pb and In+In collisions at the CERN SPS. [Lourenço, RV, Wöhri] Right: The value of  $\sigma_{\text{abs}}$  as a function of  $\sqrt{s_{NN}}$ . The points show the energies used here. The line is meant to guide the eye.

# $J/\psi$ $p + \text{Pb}$ distributions as a function of $y$ and $p_T$ : Including Cold Nuclear Matter Effects

Here the  $p_T$  distribution is taken in the range  $0 < |y| < 1$  for  $p_{\text{lab}} = 40$  and 800 GeV and  $1.1 < |y| < 2.2$  for  $\sqrt{s_{NN}} = 200$  GeV

An enhanced  $k_T$  broadening is assumed for  $p + \text{Pb}$  collisions

The  $A$  dependence of intrinsic charm suppresses its contribution in the lead nucleus

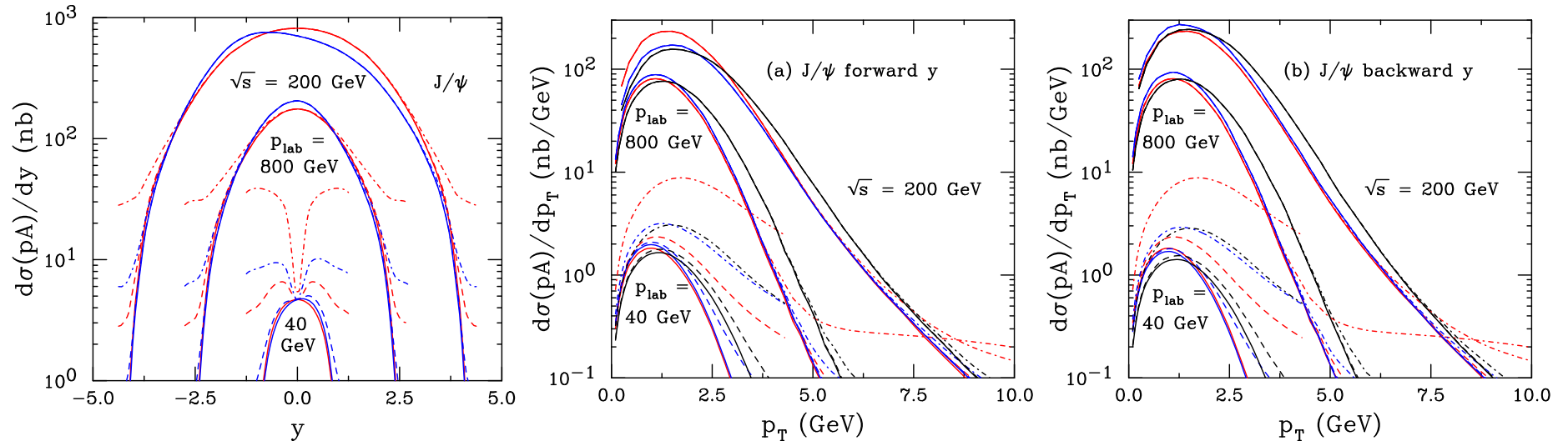


Figure 19: The  $J/\psi$  distributions at  $p + p$  and  $p + \text{Pb}$  (per nucleon) at  $p_{\text{lab}} = 40$  and 800 GeV and  $\sqrt{s} = 200$  GeV as a function of rapidity (left) and forward (middle, a) and backward (right, b) rapidity. The red curves show the results for  $p + p$  collisions while the blue and black curves show the  $p + \text{Pb}$  distributions without and with an enhanced intrinsic  $k_T$  kick respectively. (The rapidity distributions are independent of the kick.) Three curves are shown in each case: no intrinsic charm (pQCD only, solid);  $P_{\text{ic}5}^0 = 0.1\%$  (dashed); and  $P_{\text{ic}5}^0 = 1\%$  (dot-dashed). No  $J/\psi$  absorption by nucleons is considered in the  $p + \text{Pb}$  calculation.

# Summary of Previous Fixed-Target $J/\psi$ Data

**NA60**  $p_{\text{lab}} = 158$  and  $400$  GeV, covering  $0.05 < x_F < 0.4$  and  $-0.075 < x_F < 0.125$  respectively, were taken on Be, Al, Cu, In, W, Pb, and U targets (PLB 706, 263 (2012))

**NA3**  $p_{\text{lab}} = 200$  GeV,  $x_F > 0$ , taken on a Pt target (Z. Phys. C 20, 101 (1983))

**NA50**  $p_{\text{lab}} = 450$  GeV, midrapidity ( $-0.1 < x_F < 0.1$ ), used Be, Al, Cu, Ag, W and Pb targets (EPJ C 33, 31 (2004))

**E866**  $p_{\text{lab}} = 800$  GeV,  $-0.09 < x_F < 0.95$ , used Be, Fe, and W targets (PRL 84, 3256 (2000))

**HERA-B**  $p_{\text{lab}} = 920$  GeV,  $-0.34 < x_F < 0.14$ , used C, Ti and W targets (EPJ C 60, 525 (2009))



# E866 $J/\psi$ $x_F$ and $p_T$ Distributions ( $p + p$ )

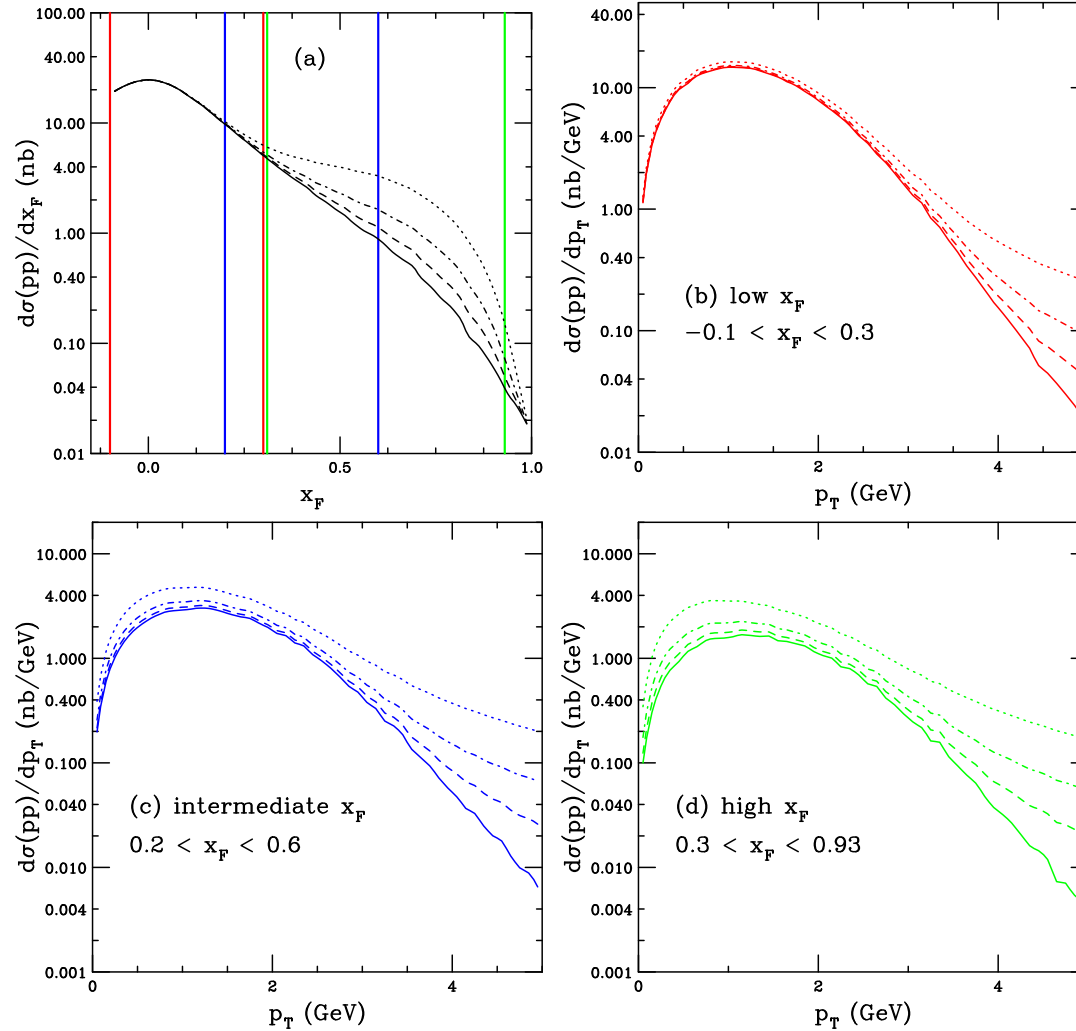


Figure 20: The  $J/\psi$  cross sections in  $p+p$  collisions at  $\sqrt{s} = 38.8$  GeV with and without IC as a function of  $x_F$  (a) and  $p_T$  at low (b), intermediate (c), and high  $x_F$  (d). The solid curves do not include IC while the dashed, dot-dashed and dotted curves use  $P_{ic5}^0 = 0.1\%$ ,  $0.31\%$  and  $1\%$  respectively. The colored vertical bars on the  $x_F$  distributions show the  $x_F$  limits of the  $p_T$  distributions in (b)-(d) and matches the color of the curves in (b)-(d). RV, PRC **103**, 035204 (2021).

# Comparison with $\alpha$ Extracted from E866 $J/\psi$ $p + A$ Data

E866 obtained  $\alpha$  as a function of  $x_F$  and  $p_T$  (in 3  $x_F$  bins) for  $A = \text{Be, Fe, and W}$

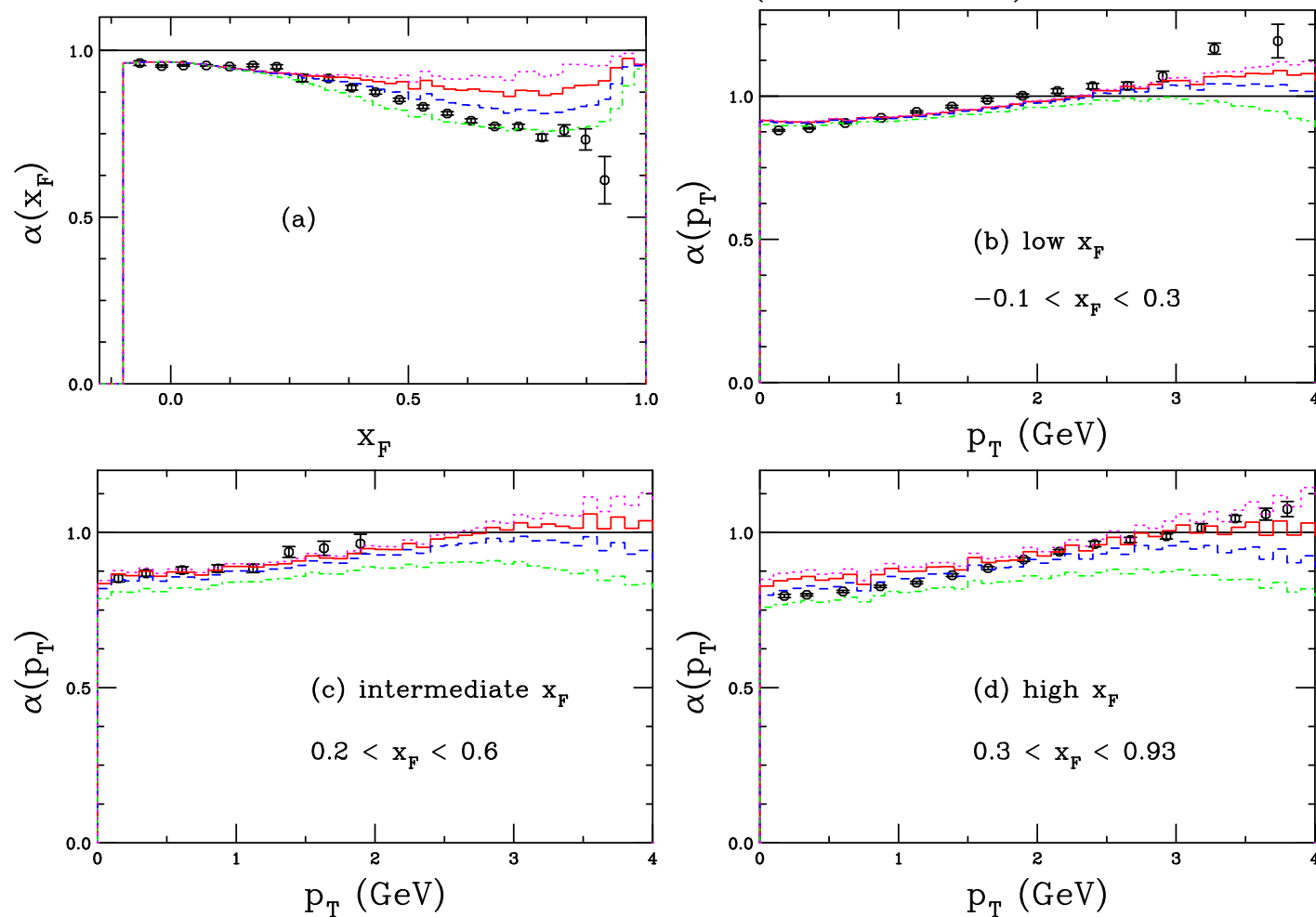


Figure 21: The exponent  $\alpha(x_F)$  (a) and  $\alpha(p_T)$  for low  $x_F$  (b), intermediate  $x_F$  (c), and high  $x_F$  (d). The dotted magenta curves use  $P_{\text{ic5}}^0 = 0$  while the solid red, dashed blue, and dot-dashed green curves show  $P_{\text{ic5}}^0 = 0.1\%$ ,  $0.31\%$  and  $1\%$  respectively. The E866 data (PRL **84**, 3256 (2000)) are the black points. From: RV, PRC **103**, 035204 (2021).

# Comparison of $\alpha(x_F)$ with Fixed-Target $J/\psi$ Data

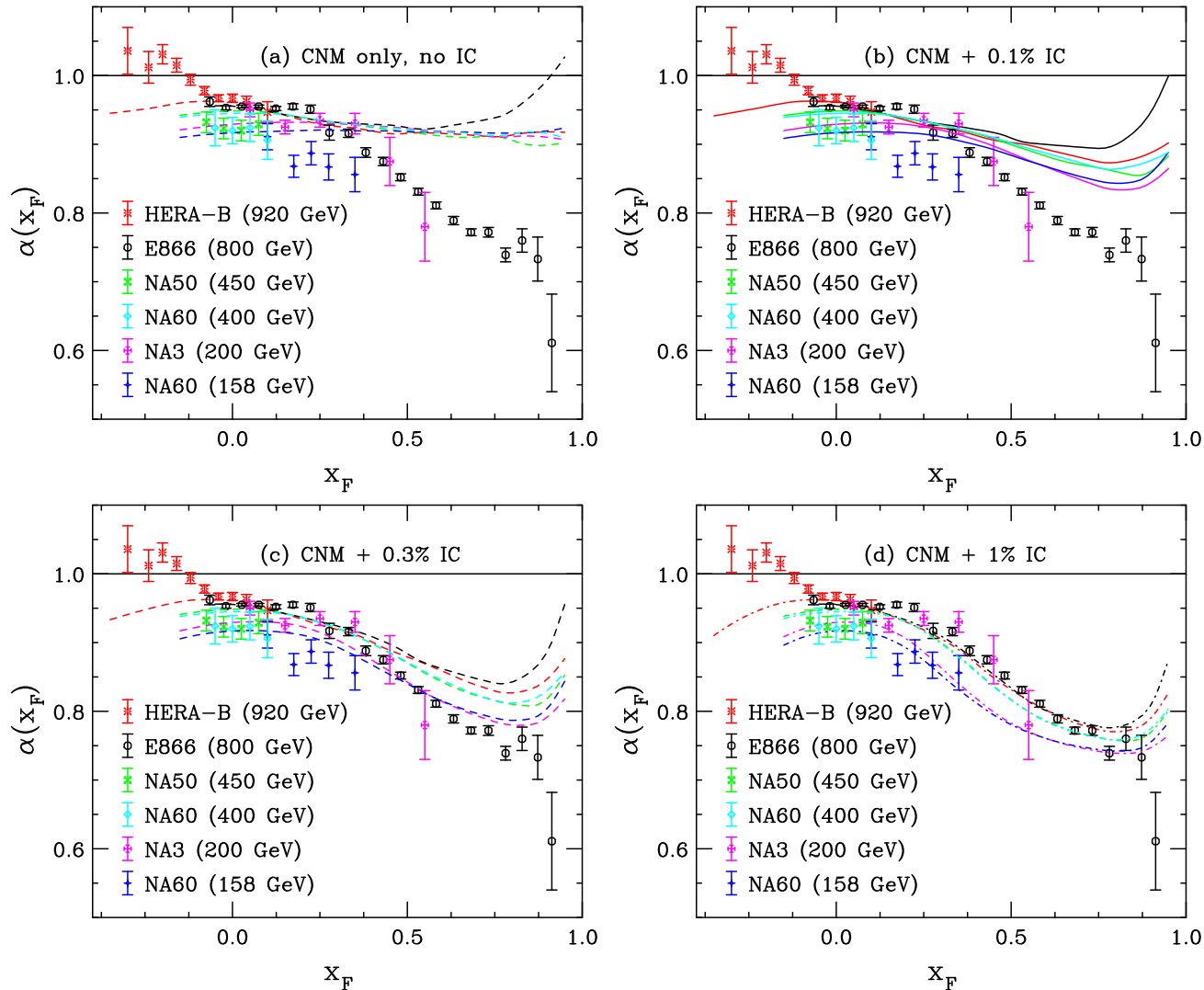


Figure 22: The value of  $\alpha(x_F)$  for  $J/\psi$  production at: NA60 ( $p_{\text{lab}} = 158$  GeV), NA3 ( $p_{\text{lab}} = 200$  GeV), NA60 ( $p_{\text{lab}} = 400$  GeV), NA50 ( $p_{\text{lab}} = 450$  GeV), E866 ( $p_{\text{lab}} = 800$  GeV), and HERA-B ( $p_{\text{lab}} = 920$  GeV). The points and curves of the same color are at the same energy. Calculations with  $P_{\text{ic}5}^0 = 0$  are in (a) while  $P_{\text{ic}5}^0 = 0.1\%$ ,  $0.3\%$ , and  $1\%$  are shown in (b)-(d).

# SeaQuest Results for $p + W$ Interactions

The large  $x_F$  contribution from intrinsic charm changes the  $x_F$  dependence from effectively flat to decreasing with  $x_F$

Enhanced  $k_T$  broadening evident with no intrinsic charm, effect is reduced when IC is included

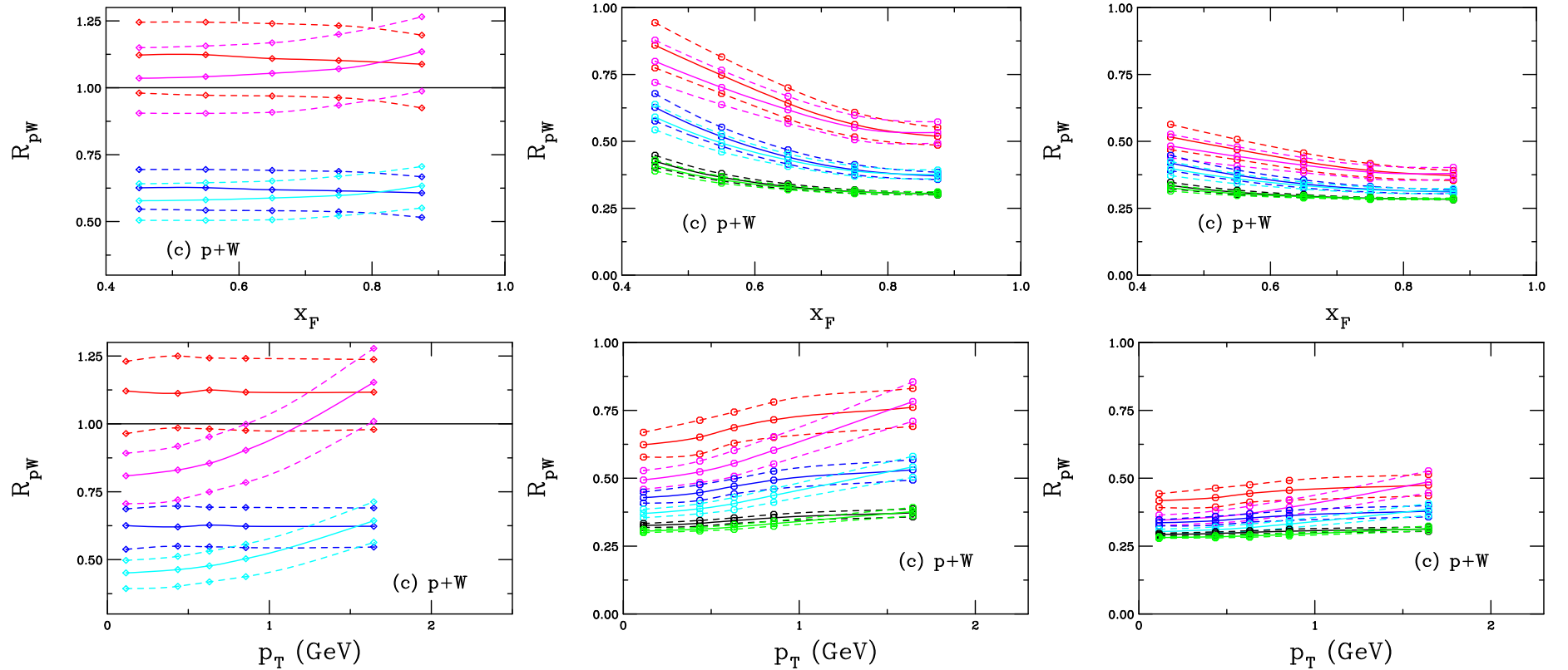


Figure 23: Left: no IC, red: EPPS16 only; magenta: EPPS16 +  $k_T$  broadening; blue and cyan, adding  $\sigma_{\text{abs}} = 9$  mb. Middle: solid lines: EPPS16 + IC; dashed: including  $k_T$  broadening;  $P_{\text{ic},5}^0 = 0.1\%$  (red, magenta),  $0.31\%$  (blue, cyan),  $1\%$  (green, black). Right: Same as middle but with  $\sigma_{\text{abs}} = 9$  mb

# SMOG $\bar{D}^0$ Results Compared to Calculations

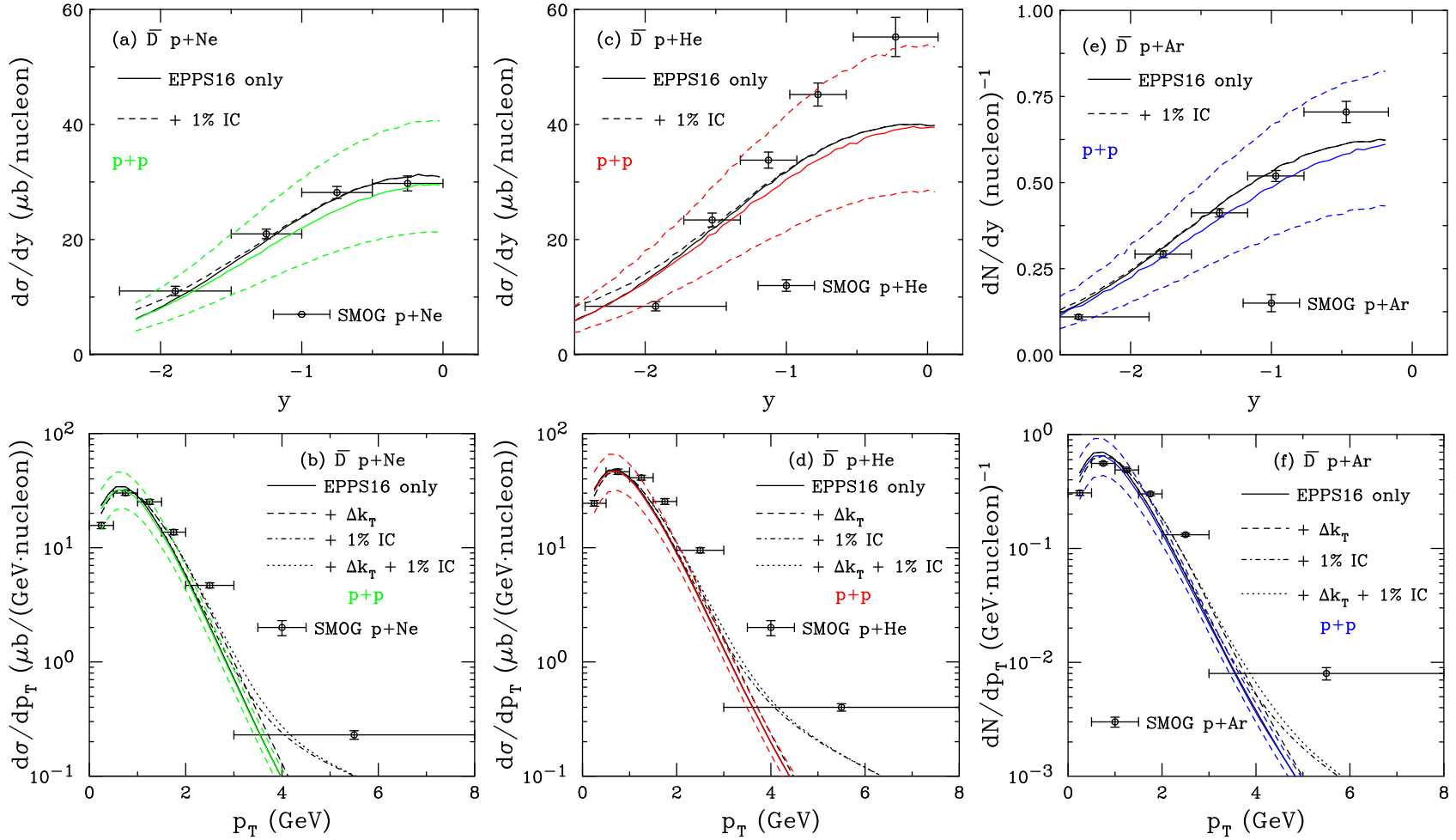


Figure 24: The  $\bar{D}$  cross section as a function of  $y$  in (a), (c), (e) and  $p_T$  in (b), (d), (f) for  $p + \text{Ne}$  ( $\sqrt{s_{NN}} = 68.5$  GeV) in (a) and (b);  $p + \text{He}$  ( $\sqrt{s_{NN}} = 86.6$  GeV) in (c) and (d); and  $p + \text{Ar}$  ( $\sqrt{s_{NN}} = 110.4$  GeV) in (e) and (f). The black curves are the  $p + A$  calculations. The colored curves (solid and dashed) show the QCD  $p + p$  calculations (no IC). The  $p + A$  rapidity distributions are shown for EPPS16 only (solid) and EPPS16 with  $P_{\text{ic}5}^0 = 1\%$  (dashed). The  $p_T$  distributions show EPPS16 only (solid); EPPS16 with  $k_T$  kick (dashed); EPPS16 and  $P_{\text{ic}5}^0 = 1\%$  (dot-dashed); and EPPS16,  $k_T$  kick and  $P_{\text{ic}5}^0 = 1\%$  (dotted). The  $p + \text{Ne}$  data are from arXiv:2211.11633; the  $p + \text{He}$  and  $p + \text{Ar}$  data are from PRL **122**, 132002 (2019).

# SMOG $J/\psi$ Results Compared to Calculations

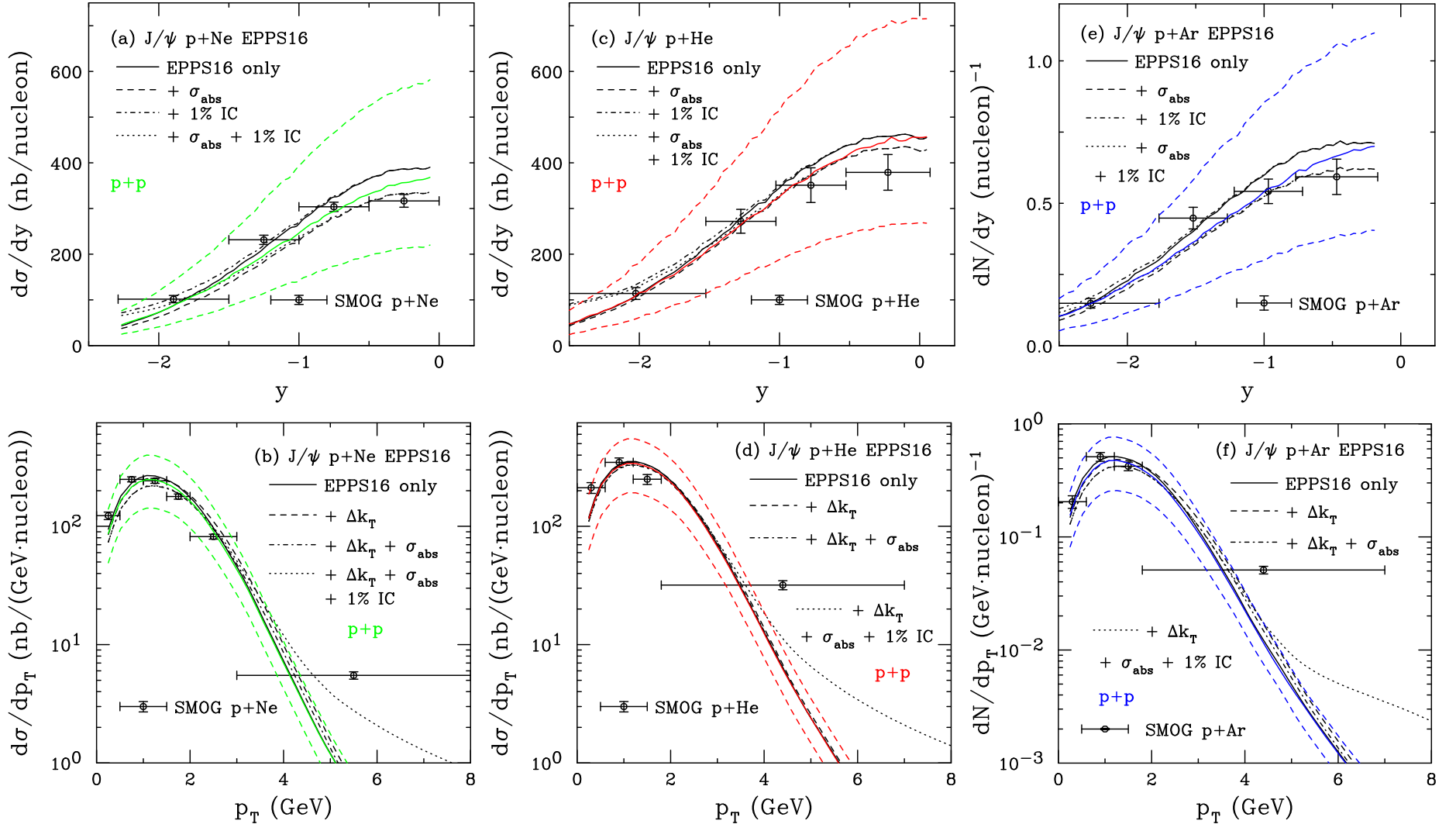


Figure 25: The  $J/\psi$  cross section as a function of  $y$  in (a), (c), (e) and  $p_T$  in (b), (d), (f) for  $p+Ne$  ( $\sqrt{s_{NN}} = 68.5$  GeV) in (a) and (b);  $p+He$  ( $\sqrt{s_{NN}} = 86.6$  GeV) in (c) and (d); and  $p+Ar$  ( $\sqrt{s_{NN}} = 110.4$  GeV) in (e) and (f). The black curves are the  $p+A$  calculations. The colored curves (solid and dashed) show the CEM  $p+p$  calculations (no IC). The  $p+A$  rapidity distributions are shown for EPPS16 only (solid); EPPS16 with absorption (dashed); EPPS16 and  $P_{ic5}^0 = 1\%$  (dot-dashed); and EPPS16, absorption, and  $P_{ic5}^0 = 1\%$  (dotted). The  $p_T$  distributions show EPPS16 only (solid); EPPS16 with  $k_T$  kick (dashed); EPPS16, absorption, and  $k_T$  kick (dot-dashed); and EPPS16, absorption,  $k_T$  kick and  $P_{ic5}^0 = 1\%$  (dotted). The  $p+Ne$  data are from arXiv:2211.11645; the  $p+He$  and  $p+Ar$  data are from PRL **122**, 132002 (2019).

# Asymmetries Between $\bar{D}^0$ and $D^0$ Mesons: Leading vs. Non-leading Charm

Assuming 1% IC for leading  $\bar{D}^0(\bar{c}u)$  and no IC for non-leading  $D^0(c\bar{u})$  underestimates the measured  $p + \text{Ne}$  asymmetry (SMOG defined asymmetry as  $c - \bar{c}$ , not as leading vs. non-leading)

No obvious reason why IC would give finite asymmetry at  $y \sim 0$

Maciula and Szczurek included production by recombination with IC which gives larger asymmetry at finite  $y$  but no asymmetry at large  $p_T$

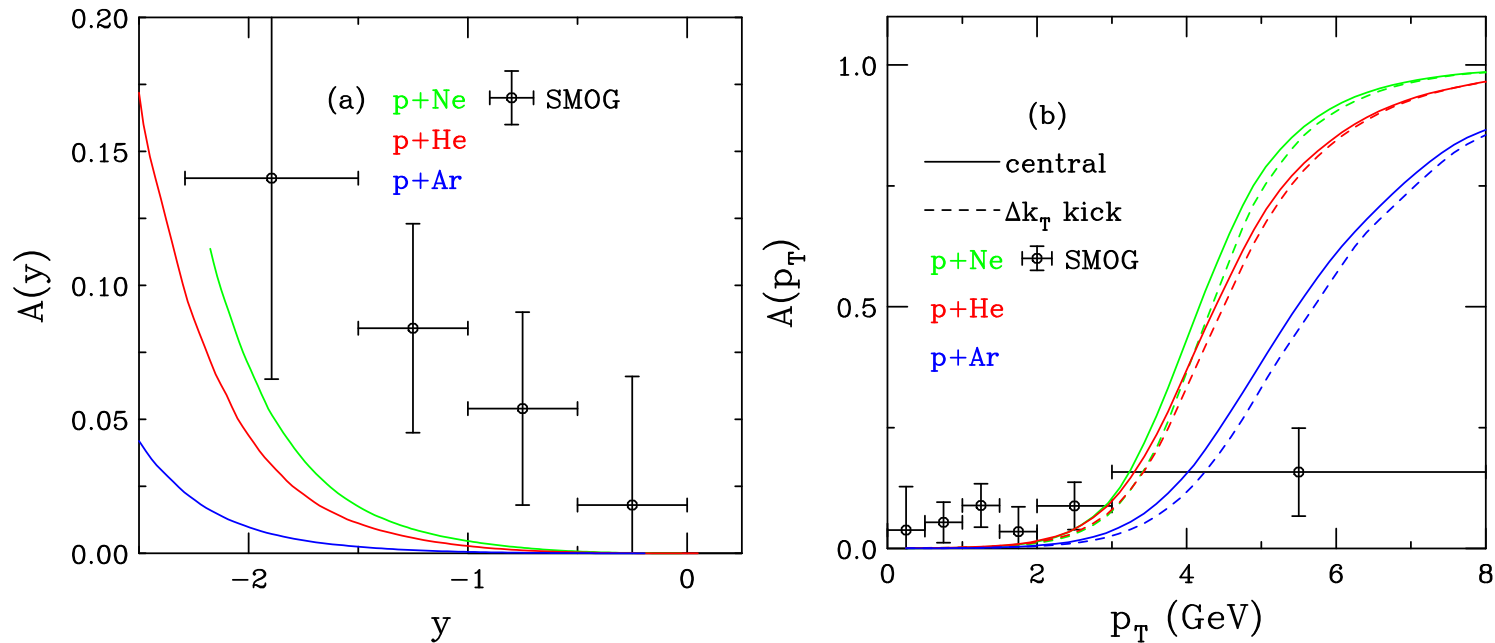


Figure 26: The  $\bar{D}$ - $D$  asymmetry as a function of rapidity (a) and transverse momentum (b) for  $p + \text{Ne}$  collisions at  $\sqrt{s_{NN}} = 68.5$  GeV (green);  $p + \text{He}$  collisions at  $\sqrt{s_{NN}} = 86.6$  GeV (red); and  $p + \text{Ar}$  collisions at  $\sqrt{s_{NN}} = 110.4$  GeV (blue). All calculations include the EPPS16 central set and  $P_{ic5}^0 = 1\%$ . In (b) the dashed curves also include a  $k_T$  kick. Data from arXiv:2211.11633.

# Summary

Intrinsic charm, new in the 1980's is experiencing a renaissance of new interest  
Model calculations in good agreement with the SMOG  $p + A$  cross section data but underestimates asymmetry; more precise data needed at backward rapidity and high  $p_T$   
Other fixed-target data, as from NA60+, would be useful to study potentially larger IC contributions closer to midrapidity  
Charm measurements at the EIC, to be built at Brookhaven National Lab in the US, could potentially study forward charm (lower energy than HERA so it could be observable)  
IC may also be useful for studying exotic hadron structure: studies with  $|uud\bar{b}\bar{b}\bar{b}\bar{b}\rangle$  states showed that the proposed double  $\Upsilon$  state reported (average mass 18.15 GeV) by the A<sub>N</sub>DY Collaboration was smaller than calculated mass of the state but compatible with proposed  $\bar{b}\bar{b}\bar{b}\bar{b}$  tetraquark masses (PRD 104, 094025 (2021)); stay tuned for that